



Journal of The Ferrata Storti Foundation

## Combinatorial efficacy of entospletinib and chemotherapy in patient-derived xenograft models of infant acute lymphoblastic leukemia

by Joseph P. Loftus, Anella Yahiaoui, Patrick A. Brown, Lisa M. Niswander, Asen Bagashev, Min Wang, Allyson Schauf, Stacey Tannheimer, and Sarah K. Tasian

Haematologica 2020 [Epub ahead of print]

*Citation: Joseph P. Loftus, Anella Yahiaoui, Patrick A. Brown, Lisa M. Niswander, Asen Bagashev, Min Wang, Allyson Schauf, Stacey Tannheimer, and Sarah K. Tasian. Combinatorial efficacy of entospletinib and chemotherapy in patient-derived xenograft models of infant acute lymphoblastic leukemia.*

*Haematologica. 2020; 105:xxx*

*doi:10.3324/haematol.2019.241729*

### *Publisher's Disclaimer.*

*E-publishing ahead of print is increasingly important for the rapid dissemination of science. Haematologica is, therefore, E-publishing PDF files of an early version of manuscripts that have completed a regular peer review and have been accepted for publication. E-publishing of this PDF file has been approved by the authors. After having E-published Ahead of Print, manuscripts will then undergo technical and English editing, typesetting, proof correction and be presented for the authors' final approval; the final version of the manuscript will then appear in print on a regular issue of the journal. All legal disclaimers that apply to the journal also pertain to this production process.*

**Title: Combinatorial efficacy of entospletinib and chemotherapy in patient-derived xenograft models of infant acute lymphoblastic leukemia**

Joseph P Loftus,<sup>1\*</sup> Anella Yahiaoui,<sup>2\*</sup> Patrick A Brown,<sup>3</sup> Lisa M Niswander,<sup>1</sup> Asen Bagashev,<sup>1</sup> Min Wang,<sup>2</sup> Allyson Shauf,<sup>2</sup> Stacey Tannheimer,<sup>2</sup> Sarah K Tasian<sup>1,4</sup>

1 Children's Hospital of Philadelphia, Division of Oncology and Center for Childhood Cancer Research; Philadelphia, PA

2 Gilead Sciences; Foster City, CA

3 Johns Hopkins University and Sidney Kimmel Comprehensive Cancer Center, Department of Pediatrics, Division of Pediatric Hematology/Oncology; Baltimore, MD

4 University of Pennsylvania Perelman School of Medicine, Department of Pediatrics and Abramson Cancer Center; Philadelphia, PA

\*JPL and AY contributed equally as first authors

Running title: SYK Inhibition for Infant ALL

Corresponding author:

Sarah K Tasian, MD

Children's Hospital of Philadelphia

University of Pennsylvania Perelman School of Medicine

3501 Civic Center Boulevard, CTRB 3010

Philadelphia, Pennsylvania 19104

Phone: 267.425.0118

Fax: 215.590.3770

Email: [tasians@email.chop.edu](mailto:tasians@email.chop.edu)

Abstract word count: 250

Word count: 3787

References: 62

Tables and figures: 1 table, 6 figures

Supplemental tables and figures: 1 table, 10 figures

Presented in part at the European Hematology Association 2018 Annual Congress (Stockholm, Sweden), American Society of Hematology 2017 annual meeting (Atlanta, GA), and the European Hematology Association 2017 Annual Congress (Madrid, Spain)

Key points:

1. SYK pathway signaling is constitutively activated in infant *KMT2A*-rearranged ALL cells and can be inhibited *in vitro* by entospletinib.
2. Combined SYK inhibition with vincristine or MEK inhibition potently inhibited *in vivo* leukemia proliferation in *KMT2A*-R ALL PDX models.

## ABSTRACT

Survival of infants with *KMT2A*-rearranged acute lymphoblastic leukemia (ALL) remains dismal despite intensive chemotherapy. We observed constitutive phosphorylation of spleen tyrosine kinase (SYK) and associated signaling proteins in infant ALL patient-derived xenograft (PDX) model specimens and hypothesized that the SYK inhibitor entospletinib would inhibit signaling and cell growth *in vitro* and leukemia proliferation *in vivo*. We further predicted that combined entospletinib and chemotherapy could augment anti-leukemia effects. Basal kinase signaling activation and *HOXA9/MEIS1* expression differed among *KMT2A*-rearranged (*KMT2A-AFF1* [n=4], *KMT2A-MLLT3* [n=1], *KMT2A-MLLT1* [n=4]) and non-*KMT2A*-rearranged [n=3] ALL specimens and stratified by genetic subgroup. Incubation of *KMT2A*-rearranged ALL cells *in vitro* with entospletinib inhibited methylcellulose colony formation and SYK pathway signaling in a dose-dependent manner. *In vivo* inhibition of leukemia proliferation with entospletinib monotherapy was observed in RAS-wild-type *KMT2A-AFF1*, *KMT2A-MLLT3*, and *KMT2A-MLLT1* ALL PDX models with enhanced activity in combination with vincristine chemotherapy in several models. Surprisingly, entospletinib did not decrease leukemia burden in two *KMT2A-AFF1* PDX models with *NRAS* or *KRAS* mutations, suggesting potential RAS-mediated resistance to SYK inhibition. As hypothesized, superior inhibition of ALL proliferation was observed in *KMT2A-AFF1* PDX models treated with entospletinib and the MEK inhibitor selumetinib versus vehicle or inhibitor monotherapies (p<0.05). In summary, constitutive activation of SYK and associated signaling occurs in *KMT2A*-rearranged ALL with *in vitro* and *in vivo* sensitivity to entospletinib. Combination therapy with vincristine or selumetinib further enhanced treatment effects of SYK inhibition. Clinical study of entospletinib and chemotherapy or other kinase inhibitors in patients with *KMT2A*-rearranged leukemias may be warranted.

## INTRODUCTION

B-cell acute lymphoblastic leukemia (B-ALL) is the most common childhood cancer and is characterized by recurrent somatic cytogenetic and molecular abnormalities. While modern risk-adapted chemotherapy regimens for children and adolescents/young adults (AYAs) have achieved overall survival rates exceeding 90% (1, 2), optimal salvage therapy for the 10-15% of children and >60% of adults with B-ALL who relapse remains a major unmet medical need (3-5).

Patients with B-ALL harboring rearrangements in *lysine-specific methyltransferase 2A* (*KMT2A*, formerly *mixed lineage leukemia* [*MLL*]; located at chromosome 11q23) are at higher risk of relapse and have inferior overall survival (6-8). *KMT2A* rearrangements occur in approximately 10% of childhood and adult B-ALL cases with highest frequency (75%) in infants diagnosed with leukemia at <365 days old (8, 9). Children with *KMT2A*-rearranged (*KMT2A*-R) ALL have poor prognoses with 5-year event-free survival (EFS) of 20-50% in infants (9-12) and approximately 58% in older children (13). Age <6 months at diagnosis, hyperleukocytosis with white blood cell count greater than 300,000 cells/uL, and poor response to prednisone prophase chemotherapy have been associated with worst clinical outcomes and dismal long-term survival amongst infants with *KMT2A*-R ALL (10, 11). Adults with *KMT2A*-R ALL have similarly poor outcomes with <50% 5-year EFS (14).

Wild-type *KMT2A* is required for normal hematopoiesis and post-natal hematopoietic cell maintenance (15). Disruption of *KMT2A* via chromosomal translocation in acute lymphoid and myeloid leukemias was first described nearly three decades ago (16, 17). In ALL, these translocations result in fusion of *KMT2A* to one of >100 currently known translocation partner genes, leading to production of fusion proteins which disrupt normal regulation of gene expression by wild-type *KMT2A* (18-20). Recruitment of the super elongation complex (SEC) and the H3K79 histone methyltransferase DOT1L by the fusion proteins consequently leads to new fusion-dependent functions of *KMT2A* (21). While numerous partner genes have been

reported, five translocations account for the majority of *KMT2A* rearrangements in ALL across the age spectrum. These include t(4;11)(q21;q23) with *KMT2A-AFF1* fusion (60%), t(11;19)(q23;p13.3) with *KMT2A-MLLT1* fusion (18%), t(9;11)(p21;q23) with *KMT2A-MLLT3* fusion (12%), t(10;11)(p12;q23) with *KMT2A-MLLT10* fusion (3%), and t(6;11)(q27;q23) with *KMT2A-MLLT4* fusion (1%) (8, 22-24).

Preclinical studies of murine models and primary patient specimens demonstrate that *KMT2A-R* ALL cells harbor gene expression signatures with distinct arrest in B cell development at the pro-B and pre-B cell stages. Recent publications have reported a strong link between increased expression of the HOX cluster of transcription factor genes (particularly *HOXA9*) and its cofactor *MEIS1* in accelerating *KMT2A-R* leukemia development via upregulation of spleen tyrosine kinase (SYK) (21, 25), as well as constitutive activation of SYK signaling in several B-ALL subtypes (2, 26). The specific mechanisms by which *KMT2A* translocations contribute to SYK signaling in B-ALL and their role in leukemogenesis and maintenance remain incompletely characterized.

SYK is expressed in hematopoietic cells and involved in multiple signal transduction pathways downstream of the B cell receptor (BCR). SYK is autophosphorylated and activated when its two tandem Src homology 2 (SH2) domains bind to immunoreceptor tyrosine based activation motifs (ITAMs) (27). This binding then initiates downstream signal transduction via activation of effector molecules, including phospholipase C gamma (PLC $\gamma$ ), B cell linker protein (BLNK), phosphatidylinositol 3 kinase (PI3K), and mitogen activated protein kinase (MAPK), that converge to activate multiple downstream signaling pathways involved in B cell malignancies, thereby making SYK an attractive potential therapeutic target (28, 29). *In vitro* and *in vivo* activity of SYK inhibition in preclinical B-ALL models has been previously established (30-32), and several SYK inhibitors (*e.g.*, entospletinib, fostamatinib) are being evaluated in patients with relapsed/refractory solid tumors, hematologic malignancies, or autoimmune diseases.

Entospletinib (ENTO, formerly GS-9973 (33)) is a potent and highly selective SYK inhibitor under current clinical investigation in adults with relapsed acute leukemias (NCT02343939, NCT02404220). Interim analysis of a phase 1b/2 study of ENTO and chemotherapy showed complete responses in two patients with relapsed *KMT2A*-R acute myeloid leukemia (AML) treated with ENTO monotherapy for 14 days, suggesting potential for particular clinical activity in *KMT2A*-rearranged leukemias (34). Translating the efficacy of SYK inhibition with ENTO and depth of response in combination with standard-of-care chemotherapy agents warrants further investigation at a molecular level. In the current study, we assessed the therapeutic potential of ENTO monotherapy and in combination with chemotherapy or other kinase inhibitors in preclinical infant *KMT2A*-R and non-*KMT2A*-R ALL patient-derived xenograft (PDX) models to delineate the potential anti-leukemic utility of SYK inhibition in this high-risk childhood leukemia subtype.

## **METHODS**

### *KMT2A-rearranged ALL patient specimens and xenotransplantation models*

Viably cryopreserved leukemia cells from infants with *de novo* *KMT2A*-R (n=4; corresponding relapse, n=3) and non-*KMT2A*-R ALL (n=3) enrolled on the Children's Oncology Group (COG) trial AALL0631 were obtained via informed consent as described (35). Additional specimens from an infant with relapsed *KMT2A*-R (n=1; ALL3103) and an adult with *de novo* *KMT2A*-R ALL (n=1; ALL3113) were obtained from the University of California, San Francisco and University of Pennsylvania leukemia biorepositories under approved institutional research protocols after informed consent in accordance with the Declaration of Helsinki (**Table 1**). Patient-derived xenograft (PDX) models were established in NOD.Cg-Prkdcscid Il2rgtm1Wjl/SzJ (NSG) mice via an Institutional Animal Use and Care Committee-approved protocol at the Children's Hospital of Philadelphia as described with serial transplantation of human ALL cells into secondary or tertiary recipients for experimental studies (36-39). Additional established non-

*KMT2A-R* ALL PDX models (primarily of the Philadelphia chromosome-like [Ph-like] subtype (15, 38-40); **Supplemental Table 1**) were used as negative controls.

#### *Kinase inhibitors and chemotherapy*

The selective SYK inhibitor entospletinib (ENTO) (33) was provided as a dispersible powder for *in vitro* studies and in rodent chow formulation in 0.03%, 0.05%, and 0.07% concentrations for *in vivo* animal studies by Gilead Sciences, Inc. (Foster City, CA). Rodent chow concentrations were selected and optimized based upon PK levels achieved in ENTO-treated adult patients with acute leukemia (NCT02404220, NCT02343939) (34). Vincristine and dexamethasone were purchased from the Children's Hospital of Philadelphia investigational pharmacy (Philadelphia, PA). The MEK inhibitor selumetinib, SYK inhibitor fostamatinib, and multi-kinase inhibitor dasatinib were purchased from Selleckchem (Houston, TX) or LC Labs (Woburn, MA). Cell viability and phosphoflow cytometry signaling analyses of human B-ALL cell lines and PDX model cells treated with vehicle, kinase inhibitors, or chemotherapy (*in vitro* or *in vivo*) are detailed in Supplemental Methods with data shown in **Supplemental Figures 1-6**.

#### *In vivo drug testing in patient-derived xenograft (PDX) models*

Animal studies were conducted under a CHOP Institutional Animal Use and Care Committee (IACUC)-approved protocol in accordance with the Panel on Euthanasia of the American Veterinary Medical Association's guidelines. After flow cytometric (FC) confirmation of  $\geq 1\%$  CD45<sup>+</sup> CD19<sup>+</sup> human ALL (fluorochrome-conjugated antibodies from EBioscience) in murine peripheral blood, engrafted ALL PDX models were randomized to treatment with vehicle, ENTO chow orally *ad libitum*, vincristine 0.1 mg/kg intraperitoneally (IP) weekly, or both ENTO and vincristine for 72 hours (pharmacokinetic [PK] and pharmacodynamics [PD] studies) or up to 28 days (treatment efficacy studies) as described (38, 39). Vincristine dosing was previously optimized in ALL cell line and PDX models (not shown). Additional studies in some ALL PDX

models assessed selumetinib 100 mg/kg administered orally twice daily(41) 5 days/week as (ALL135MR and ALL3113) or dexamethasone 1 mg/kg PO once daily 5 days/week (ALL3113, ALL83GD) as monotherapy or in combination with ENTO. Further details about *in vivo* drug testing in ALL PDX models and conduction of all other experimental studies are included in the Supplemental Methods.

## RESULTS

### *Characterization of constitutive SYK pathway activation in infant KMT2A-R ALL PDX models*

Constitutive SYK pathway activation was detected across a genetic spectrum of infant ALL and some non-infant Philadelphia chromosome-like (Ph-like) ALL control specimens using harvested murine spleens from well-engrafted PDX models (**Table 1**). Assessment of phosphorylated and total SYK levels revealed that expression of high basal phosphorylated SYK (pSYK) was seen in the majority of infant non-*KMT2A-R* and *KMT2A-R* ALL specimens (**Figure 1**, left). pSYK levels were also elevated in some Ph-like ALL specimens and absent in splenic tissue from non-leukemia-injected NSG mice (**Figure 1**, right). Total SYK expression was relatively consistent across all models. The observed constitutive basal pSYK levels, coupled with a previously suggested role of upregulated SYK as a driver in AML models with high *HOXA9* and *MEIS1* expression (25), and early reports of clinical responses in adults with relapsed *KMT2A-R* leukemias treated with entospletinib (42, 43) led us to investigate the role of SYK signaling and therapeutic potential of ENTO specifically in infant *KMT2A-R* ALL PDX models.

### *Entospletinib decreases leukemic burden and inhibits kinase signaling in KMT2A-R ALL*

SYK plays a pivotal role upstream of several key leukemia-associated signaling pathways (26, 29), including RAS/MAPK, PI3K/AKT/mTOR, and JAK/STAT. SYK inhibition by ENTO has the potential to impact multiple signal transduction pathways in ALL (**Visual**

**Abstract**), leading to potential anti-leukemic efficacy. Given our initial demonstration of constitutive SYK and other signaling pathway activation in infant ALL specimens by Simple Western, we first assessed leukemia cell growth inhibitory effects of ENTO *in vitro* using methylcellulose colony assays. Viably cryopreserved harvested *KMT2A-R* PDX ALL cells (model ALL3103 with *KMT2A-MLLT3* fusion) were grown under anchorage-independent (non-adherent) conditions in serum-free methylcellulose and treated with a clinically-relevant dose range of ENTO for 14 days (**Figure 2A**). ENTO maximally inhibited colony formation (89% inhibition;  $p < 0.0001$  by t-test), suggesting that SYK plays a central role upstream of signaling pathways necessary for proliferation and survival.

We then assessed the ability of ENTO to inhibit leukemia proliferation *in vivo* in ALL3103 and NH011 (Ph-like ALL with *NUP214-ABL1* fusion) PDX mice. ENTO 0.03% and 0.07% chow concentrations administered for 28 days both potently decreased human CD45+ CD19+ ALL cell counts in peripheral blood measured weekly by quantitative flow cytometry and in end-study spleens (**Figure 2B-C** and **Supplemental Figure 7**). Terminal PK evaluation of ENTO in the periphery confirmed that high levels of ENTO could be achieved by continuous chow administration (**Figure 2D**) without statistical difference between the 0.03% and 0.07% treatment groups. Simple Western analysis of highly leukemia-engrafted splenic lysates from individual ENTO-treated mice demonstrated marked inhibition of pSYK Y323, cMYC and pERK T202/Y204 as compared to control chow-treated animals after 4 weeks of treatment (**Figure 2E**) and high correlation between ENTO levels and pSYK and pERK inhibition in well-engrafted ALL3103 PDX mice treated in pharmacodynamic studies for 72 hours with entospletinib (**Supplemental Figure 8**). These results confirmed the on-target inhibition of pSYK and key downstream signaling phosphoproteins by ENTO, suggesting that an achieved dose level of 3330-7900 nM *in vivo* was sufficient to inhibit constitutive pSYK signaling and decrease *in vivo* leukemia proliferation in an aggressive relapsed infant *KMT2A-R* ALL PDX model.

### *In vitro pharmacodynamic inhibition of signaling proteins in infant KMT2A-R models*

To extend our observation of ALL cell SYK dependency for proliferation and survival in other *KMT2A-R* fusion types, we evaluated ENTO in another aggressive multiply-relapsed infant ALL PDX model with *KMT2A-MLLT1* fusion (ALL135MR) in short-term *in vitro* cultures and observed dose-dependent inhibition of pERK1/2, pAKT<sup>S473</sup>, pSTAT5, and cMYC (**Figure 3A**). Interestingly, similar *in vitro* incubation of leukemia cells from an infant ALL PDX model with *KMT2A-AFF1* fusion and concomitant *NRAS*<sup>G12D</sup> mutation (ALL142MR) with ENTO showed little to no inhibition of the same key pathways (**Figure 3B**). These data suggest differential signaling effects potentially related to specific *KMT2A* fusion partner and/or RAS-mutant status.

### *Evaluation of expression signatures in KMT2A-R ALL subtypes*

*KMT2A-R* ALL has been shown to have distinct gene expression signatures that define B-cell developmental arrest at either the pro-B and pre-B cell stages (22). Understanding the signaling pathway dependencies of different *KMT2A-R* fusion proteins in infant ALL cells may lead to more effective therapeutic targeting strategies for this high-risk patient population. To assess potential differential gene expression signatures, we evaluated the transcription factors *HOXA9* and *MEIS1*, which are known downstream targets of *KMT2A*. As hypothesized, *HOXA9* and *MEIS1* expression levels correlated with both *KMT2A-R* fusion status and specific gene partner (**Figure 4A**). Infant ALL specimens with *KMT2A-MLLT3* and *KMT2A-MLLT1* fusions expressed both high *HOXA9* and *MEIS1*, while *KMT2A-AFF1* models had high *MEIS1* and normal *HOXA9* expression. Conversely, infant non-*KMT2A-R* samples had normal expression levels of *HOXA9* and *MEIS1*. These distinct expression signatures exhibited amongst *KMT2A-R* samples with different fusion partners are concordant with reports of differential chromatin binding of *KMT2A-R* fusion proteins leading to distinct gene expression profiles and potentially differential clinical outcomes (1, 21).

Given the observed stratification of *HOXA9* and *MEIS1* expression signatures among the *KMT2A* subgroups, we next assessed protein expression signatures in these samples to evaluate potential correlation. Simple Western analysis of splenic lysates from *KMT2A*-R and non-*KMT2A*-R ALL PDX models (**Figure 4B**) demonstrated that leukemias with different *KMT2A* fusion partners induced different patterns of signaling activation. High levels of cMYC were detected only in *KMT2A-AFF1* models, while *KMT2A-MLLT1* models had high SRC, absent PTEN, and high pAKT levels. Regulation of both SRC and PI3K pathways are known to be potentially SYK-dependent, concordant with data from our *in vitro* studies in ENTO-treated ALL135MR cells (**Figure 3A**). Overall, differential gene expression signatures between *KMT2A*-R and non-*KMT2A*-R ALL subtypes (**Supplemental Figure 9A**) and differences between gene and protein expression signatures among the *KMT2A* fusion subtypes (**Supplemental Figure 9B, Figure 4B**) showed unique signaling dependencies that may relate to their differential ENTO sensitivity.

*Entospletinib potently inhibits in vivo ALL proliferation with enhanced efficacy in combination with chemotherapy*

We then investigated the extent to which ENTO could inhibit *in vivo* leukemia proliferation in ALL PDX models when administered as monotherapy or in combination with vincristine (VCR) chemotherapy. We observed that combined ENTO and VCR treatment resulted in superior inhibition of ALL proliferation in a *KMT2A-MLLT3* (ALL3103) model and a *KMT2A-MLLT1* (ALL135MR) model (both RAS wild-type) than was observed with single-agent ENTO or VCR (**Figure 5A**;  $p < 0.001$  and  $p < 0.05$ , respectively). Superior leukemic cell depletion with ENTO and VCR combination was confirmed by quantitative CD19 IHC in harvested murine spleens and bone marrow (representative ALL3103 data shown in **Supplemental Figure 10**). Conversely, drug treatment of two RAS-mutant *KMT2A*-R ALL PDX models (**Figure 5B**) showed marked vincristine-induction reduction of leukemic burden (ALL142MR,  $p < 0.0001$ ;

ALL150MD,  $p < 0.001$ ), but no effects of ENTO monotherapy or additional treatment effect of combined ENTO and VCR. Evaluation of an adult RAS wild-type *KMT2A-AFF1* ALL PDX model (ALL3113) showed significant treatment effects of ENTO alone and in combination with VCR ( $p < 0.0001$  for both) (**Figure 5C**), contrasting with effects observed in the RAS-mutant models. Taken together, these data indicate that RAS mutations in *KMT2A-R* subtypes may overcome or prevent potential anti-leukemia activity of ENTO.

We then explored treatment effects of ENTO in a control non-*KMT2A-R* ALL PDX model with  $t(1;19)$  resulting in *TCF3-PBX1* fusion and a *KRAS*<sup>G12D</sup> mutation (ALL132GD), which we expected to be sensitive to ENTO given typical pre-BCR expression on this more mature B-ALL subtype (44, 45) and confirmed by positive FC immunoglobulin  $\mu$ -heavy chain staining on AALL132GD cells (not shown). However, we saw no response to single-agent ENTO or in combination with VCR, further substantiating the potential impact of RAS mutations upon ENTO insensitivity (**Figure 5D**). Finally, we tested ENTO and VCR in two RAS wild-type non-*KMT2A-R* ALL PDX models (ALL185GD and ALL83GD; **Figure 5E**). We observed sensitivity of model ALL185GD to ENTO monotherapy ( $p < 0.05$ ) and in combination with VCR ( $p < 0.0001$ ), although latter effects were not different from those of VCR monotherapy. Model ALL83GD was not sensitive to ENTO alone, but showed significant combinatorial treatment efficacy versus ENTO or VCR monotherapy ( $p < 0.0001$  and  $p < 0.05$ , respectively). Interestingly, we discovered that the ALL185GD and ALL83GD non-*KMT2A-R* models have *P2RY8-CRLF2* fusions with expected constitutive activation of JAK/STAT signaling (**Figure 4B**). Our group recently reported an essential role of SFK signaling in *CRLF2*-rearranged Ph-like ALL with *in vitro* and *in vivo* sensitivity to the kinase inhibitor dasatinib (46, 47) and hypothesize that the observed ENTO sensitivity in our *CRLF2-R* infant ALL models could be due to a similar mechanism and signaling dependency.

### *Superior preclinical activity of combined SYK and MEK inhibition in KMT2A-R ALL PDX models*

Given the surprising observed lack of ENTO activity in our RAS-mutant *KMT2A-AFF1* infant ALL PDX models, we hypothesized that dual treatment with ENTO and a MEK inhibitor (MEKi) would have superior therapeutic effects. To test this prediction, we treated RAS-mutant (ALL142MR; infant) and RAS wild-type (ALL3113MR; adult) *KMT2A-AFF1* ALL PDX models with ENTO, selumetinib (SEL), or both kinase inhibitors and quantified ALL cell counts in peripheral blood during treatment and in end-study spleens. As expected (41, 48), single-agent SEL treatment of the RAS-mutant ALL142MR model appreciably decreased leukemia burden and augmented anti-ALL effects in combination with ENTO (**Figure 6A**). Despite its lack of RAS mutation, the ALL3113 model was surprisingly sensitive to SEL monotherapy (41, 48), and potent *in vivo* activity with near-complete leukemia clearance was observed with dual ENTO and SEL treatment (**Figure 6B**). These *in vivo* efficacy data in both RAS-mutant and wild-type models and our additional demonstration of constitutive pERK levels and *ex vivo* signaling inhibition in end-study spleens of both ALL142MR and ALL3113 models (**Figure 6C**) suggest that MEK inhibition may be a relevant therapeutic strategy for *KMT2A-R* ALL irrespective of RAS mutation status and may augment SYK inhibitor effectiveness.

## **DISCUSSION**

SYK pathway activation plays a central role in the proliferation and survival of malignant B-cells, implicating SYK as a potential therapeutic target. Preclinical studies have shown that SYK inhibition can attenuate the growth of B-ALL *in vitro* and *in vivo* regardless of pre-BCR expression or genetic subtype (26, 29). Mohr and colleagues also recently reported that *HOXA9/MEIS1*-induced upregulation of SYK is a major driver of leukemogenesis in AML (25). Several early phase clinical trials are now testing the safety and potential efficacy of ENTO in combination with chemotherapy in adults with relapsed or refractory leukemias (NCT02404220, NCT02343939, NCT03135028). Interim results from these studies have reported manageable

adverse events and remarkable response rates, particularly in patients with *KMT2A-R* AML (NCT02343939) (34).

Chemotherapy resistance and subsequent relapse remain a major cause of childhood cancer mortality, especially for infants with *KMT2A-R* B-ALL who have extremely poor event-free survival (EFS). In one study, Pieters and colleagues reported three-fold higher risk of relapse or death in infants with *KMT2A-R* ALL (irrespective of *KMT2A* rearrangement subtype) versus those without *KMT2A* rearrangements (10). Outcomes for infants with the *KMT2A-AFF1* subtype from t(4;11) are particularly poor, although differences in associated HOX family gene expression and presence or absence of reciprocal *AFF1-KMT2A* fusions may contribute to differential clinical outcomes, as shown recently by Agras-Doblas and Bueno colleagues in a large analysis of infant ALL specimens from the European cooperative groups' Interfant-99 and -06 trials (49-51) and reviewed by Slany (20).

Several groups have hypothesized that addition of targeted inhibitors to frontline chemotherapy could decrease relapse risk and improve survival for infants with ALL, as has been shown with tyrosine kinase inhibitors (TKIs) for patients with *BCR-ABL1*-rearranged (Ph+) ALL. Unfortunately, addition of the FMS-like tyrosine kinase 3 inhibitor (FLT3i) lestaurtinib did not improve EFS for infants with *KMT2A-R* B-ALL (which usually have high FLT3 receptor [CD135] surface expression) in the COG trial AALL0631, which was likely in part attributable to insufficient PD target inhibition observed by correlative plasma inhibitory activity (PIA) assays (52, 53). Similarly, no appreciable efficacy of the FLT3i quizartinib (AC220) was observed in children with relapsed *KMT2A-R* ALL in the TACL2009-004 phase 1 clinical trial (NCT011411267), although complete responses occurred in 3 of 7 patients with relapsed *FLT3*-mutant AML with 94-100% FLT3 inhibition by PIA assay seen in all studied patients (54). Despite promising preclinical data (55, 56), clinical activity of DOT1L inhibitors (e.g., pinemetostat [EPZ-5676]) targeting the *KMT2A* complex was similarly disappointing in children with relapsed *KMT2A-R* leukemias (NCT02141828) (57), again potentially due to insufficient

achievable drug levels considered necessary for response. Menin inhibitors targeting the KMT2A complex have shown exciting preclinical activity and may have superior pharmacologic properties, but have not yet entered clinical testing. Finally, current or planned trials are assessing the potential activity of 5-azacytidine priming (COG AALL15P1; NCT02828358) or blinatumomab (58) specifically in infants with *KMT2A-R* ALL, but results of these approaches are not yet known.

Our current study sought to define the potential activity of the selective SYK inhibitor ENTO specifically in preclinical infant *KMT2A-R* ALL PDX models. Our demonstration of *in vitro* and *in vivo* anti-leukemia activity of ENTO with enhanced effects in combination with VCR or dexamethasone (critical and commonly-used anti-ALL chemotherapy agents) provides rationale for further evaluation of SYK inhibition as a therapeutic strategy for this high-risk leukemia subtype. Interestingly, we observed minimal activity of ENTO alone or with VCR in *KMT2A-R* leukemias harboring concomitant RAS mutations. This observation extended to a control non-*KMT2A-R* infant ALL model with a *TCF3-PBX1* fusion from t(1;19), which had a concomitant *KRAS* mutation and was also insensitive to ENTO. Prior studies have shown that RAS mutations occur significantly more frequently in infants with B-ALL, particularly in those with the most common *KMT2A-AFF1* subtype. Data remain conflicting whether ALL-associated RAS mutations confer higher relapse risk and inferior overall survival (8, 24, 59, 60).

The potential role of RAS mutations in conferring insensitivity to SYK inhibition in ALL was further extended by evaluation of ENTO in combination with the clinically-available MEK inhibitor selumetinib in two *KMT2A-R* ALL PDX models. As predicted (41, 61), we observed significant inhibition of leukemia proliferation with SEL treatment of a RAS-mutant *KMT2A-AFF1* infant ALL model with superior activity of ENTO and SEL combination. However, SEL monotherapy and combined SEL/ENTO therapy was also quite efficacious in a RAS wild-type *KMT2A-AFF1* adult ALL model with high basal pERK levels. These data contrast somewhat with earlier preclinical data from Irving *et al.* demonstrating preferential activity of SEL (monotherapy

or in combination with dexamethasone) in RAS-mutant ALL (41, 48), an approach now under clinical investigation in children with relapsed/refractory RAS-mutant ALL via the SeluDex phase 1/2 trial (NCT03705507), but are concordant with data from Kerstjens *et al* reporting preclinical MEK inhibitor activity in both RAS-mutant and wild-type ALL (61). Cremer and colleagues also recently reported that MAPK pathway activation is a major mechanism of entospletinib or fostamatinib resistance in AML and can be overcome with dual SYK and MEK inhibition (62).

In summary, our studies show constitutive activation of SYK and associated kinase signaling in preclinical infant *KMT2A-R* and childhood Ph-like ALL PDX models. We report potent *in vitro* and *in vivo* effects of selective SYK inhibition with enhanced activity with chemotherapy in non-RAS-mutant *KMT2A-R* ALL models. We also observed combinatorial activity of ENTO with the MEK inhibitor selumetinib in two *KMT2A-R* ALL PDX models with RAS mutation or pathway activation. Our findings warrant further evaluation of efficacy and toxicity of ENTO/SEL dual therapy in additional PDX models, potentially in combination with steroids or other traditional chemotherapy agents. Taken together, our preclinical studies demonstrate activity of ENTO in *KMT2A-R* ALL in combination with anti-ALL chemotherapy or MEK inhibition and suggest potential for clinical evaluation of SYK inhibitor-based therapies in children and adults with these high-risk leukemias.

## **ACKNOWLEDGEMENTS**

We acknowledge Dr Ann Forslund and Ms Chelsea Mullins formerly at Gilead Sciences for study protocol management and data analysis and Dr Emer Clarke at ReachBio Research Labs for assistance with experimental studies. We also thank Dr Christian Hurtz at the University of Pennsylvania for assistance with experimental studies and scientific discussion. These studies were supported by Gilead Sciences. Specimen banking for patients enrolled on the COG AALL0631 trial (NCT00557193) was supported by NIH/NCI U10CA180886 and U10CA098543. Infant and childhood ALL patient-derived xenograft model creation was also supported by the Gabrielle's Angel Foundation for Cancer Research Foundation, the Rally Foundation for Childhood Cancer Research, the SchylerStrong Foundation in memory of Schyler Anna Herman, the Simutis family childhood leukemia research fund in memory of Andrew David Simutis, and Team Nate and the Viands family childhood leukemia research fund in honor of Nathaniel J Viands. LMN was supported by NIH/NCI 5T32HD43021-15. SKT was supported by NIH/NCI K08CA184418 and 1U01CA232486 awards and Department of Defense Translational Team Science Award CA180683P1.

## **AUTHOR CONTRIBUTIONS**

JPL and AY designed and performed research, analysed data, and contributed to manuscript writing. PAB contributed vital new reagents and analysed and interpreted data. LMN, AB, MW, and AS performed research and analysed data. ST and SKT oversaw the study, designed research, analysed and interpreted data, and wrote the manuscript. SKT was responsible for revision of the manuscript. All authors approved the final version of the manuscript.

## **CONFLICTS OF INTEREST**

AY, MW, AS, and ST are current or former employees of Gilead Sciences and have equity ownership in Gilead Sciences. SKT received research funding from Gilead Sciences. The remaining authors declare no relevant conflicts of interest.

## REFERENCES

1. Pui CH, Yang JJ, Hunger SP, et al. Childhood Acute Lymphoblastic Leukemia: Progress through Collaboration. *J Clin Oncol*. 2015;33(27):2938-2948.
2. Geng H, Hurtz C, Lenz KB, et al. Self-Enforcing Feedback Activation between Bcl6 and Pre-B Cell Receptor Signaling Defines a Distinct Subtype of Acute Lymphoblastic Leukemia. *Cancer Cell*. 2015;27(3):409-425.
3. Nguyen K, Devidas M, Cheng SC, et al. Factors Influencing Survival after Relapse from Acute Lymphoblastic Leukemia: A Children's Oncology Group Study. *Leukemia*. 2008;22(12):2142-2150.
4. Teachey DT, Hunger SP. Predicting Relapse Risk in Childhood Acute Lymphoblastic Leukaemia. *Br J Haematol*. 2013;162(5):606-620.
5. Sun W, Malvar J, Sposto R, et al. Outcome of Children with Multiply Relapsed B-Cell Acute Lymphoblastic Leukemia: A Therapeutic Advances in Childhood Leukemia & Lymphoma Study. *Leukemia*. 2018;32(11):2316-2325.
6. Marks DI, Moorman AV, Chilton L, et al. The Clinical Characteristics, Therapy and Outcome of 85 Adults with Acute Lymphoblastic Leukemia and T(4;11)(Q21;Q23)/Mll-Aff1 Prospectively Treated in the Ukallxii/Ecog2993 Trial. *Haematologica*. 2013;98(6):945-952.
7. Behm FG, Raimondi SC, Frestedt JL, et al. Rearrangement of the Mll Gene Confers a Poor Prognosis in Childhood Acute Lymphoblastic Leukemia, Regardless of Presenting Age. *Blood*. 1996;87(7):2870-2877.
8. Winters AC, Bernt KM. Mll-Rearranged Leukemias-an Update on Science and Clinical Approaches. *Front Pediatr*. 2017;5:4.
9. Brown P. Treatment of Infant Leukemias: Challenge and Promise. *Hematology Am Soc Hematol Educ Program*. 2013;2013:596-600.
10. Pieters R, Schrappe M, De Lorenzo P, et al. A Treatment Protocol for Infants Younger Than 1 Year with Acute Lymphoblastic Leukaemia (Interfant-99): An Observational Study and a Multicentre Randomised Trial. *Lancet*. 2007;370(9583):240-250.
11. Driessen EMC, de Lorenzo P, Campbell M, et al. Outcome of Relapsed Infant Acute Lymphoblastic Leukemia Treated on the Interfant-99 Protocol [Corrigendum]. *Leukemia*. 2017;31(12):2854.
12. Brown P, Pieters R, Biondi A. How I Treat Infant Leukemia. *Blood*. 2019;133(3):205-214.
13. Vrooman LM, Blonquist TM, Harris MH, et al. Refining Risk Classification in Childhood B Acute Lymphoblastic Leukemia: Results of Dfci All Consortium Protocol 05-001. *Blood Adv*. 2018;2(12):1449-1458.

14. Lafage-Pochitaloff M, Baranger L, Hunault M, et al. Impact of Cytogenetic Abnormalities in Adults with Ph-Negative B-Cell Precursor Acute Lymphoblastic Leukemia. *Blood*. 2017;130(16):1832-1844.
15. Iacobucci I, Li Y, Roberts KG, et al. Truncating Erythropoietin Receptor Rearrangements in Acute Lymphoblastic Leukemia. *Cancer Cell*. 2016;29(2):186-200.
16. Tkachuk DC, Kohler S, Cleary ML. Involvement of a Homolog of Drosophila Trithorax by 11q23 Chromosomal Translocations in Acute Leukemias. *Cell*. 1992;71(4):691-700.
17. Gu Y, Nakamura T, Alder H, et al. The T(4;11) Chromosome Translocation of Human Acute Leukemias Fuses the All-1 Gene, Related to Drosophila Trithorax, to the Af-4 Gene. *Cell*. 1992;71(4):701-708.
18. Zangrando A, Dell'Orto MC, te Kronnie G, et al. MLL Rearrangements in Pediatric Acute Lymphoblastic and Myeloblastic Leukemias: MLL Specific and Lineage Specific Signatures [journal article]. *BMC Med Genomics*. 2009;2(1):36.
19. de Boer J, Walf-Vorderwulbecke V, Williams O. In Focus: MLL-Rearranged Leukemia. *Leukemia*. 2013;27(6):1224-1228.
20. Slany RK. MLL Fusion Proteins and Transcriptional Control. *Biochim Biophys Acta Gene Regul Mech*. 2020;1863(3):194503.
21. Lin S, Luo RT, Ptasinska A, et al. Instructive Role of MLL-Fusion Proteins Revealed by a Model of T(4;11) Pro-B Acute Lymphoblastic Leukemia. *Cancer Cell*. 2016;30(5):737-749.
22. Krivtsov AV, Armstrong SA. MLL Translocations, Histone Modifications and Leukaemia Stem-Cell Development. *Nat Rev Cancer*. 2007;7(11):823-833.
23. Meyer C, Burmeister T, Groger D, et al. The MLL Recombinome of Acute Leukemias in 2017. *Leukemia*. 2018;32(2):273-284.
24. Andersson AK, Ma J, Wang J, et al. The Landscape of Somatic Mutations in Infant MLL-Rearranged Acute Lymphoblastic Leukemias. *Nat Genet*. 2015;47(4):330-337.
25. Mohr S, Doebele C, Comoglio F, et al. Hoxa9 and Meis1 Cooperatively Induce Addiction to Syk Signaling by Suppressing Mir-146a in Acute Myeloid Leukemia. *Cancer Cell*. 2017;31(4):549-562.e11.
26. Perova T, Grandal I, Nutter LM, et al. Therapeutic Potential of Spleen Tyrosine Kinase Inhibition for Treating High-Risk Precursor B Cell Acute Lymphoblastic Leukemia. *Sci Transl Med*. 2014;6(236):236ra262.
27. Mócsai A, Ruland J, Tybulewicz VLJ. The Syk Tyrosine Kinase: A Crucial Player in Diverse Biological Functions. *Nat Rev Immunol*. 2010;10(6):387-402.
28. Efremov DG, Laurenti L. The Syk Kinase as a Therapeutic Target in Leukemia and Lymphoma. *Exp Opin Investig Drugs*. 2011;20(5):623-636.

29. Sharman J, Di Paolo J. Targeting B-Cell Receptor Signaling Kinases in Chronic Lymphocytic Leukemia: The Promise of Entospletinib. *Ther Adv Hematol*. 2016;7(3):157-170.
30. Perova T, Grandal I, Nutter LMJ, et al. Therapeutic Potential of Spleen Tyrosine Kinase Inhibition for Treating High-Risk Precursor B Cell Acute Lymphoblastic Leukemia. *Sci Transl Med*. 2014;6(236):236ra62.
31. Kohrer S, Havranek O, Seyfried F, et al. Pre-Bcr Signaling in Precursor B-Cell Acute Lymphoblastic Leukemia Regulates Pi3k/Akt, Foxo1 and Myc, and Can Be Targeted by Syk Inhibition. *Leukemia*. 2016;30(6):1246-1254.
32. Loftus JP, Yahiaoui A, Shen F, et al. Enhanced Efficacy of the Syk Inhibitor Entospletinib and Vincristine in Kmt2a-Rearranged Acute Lymphoblastic Leukemia. *HemaSphere*. 2018;2(S1):36.
33. Currie KS, Kropf JE, Lee T, et al. Discovery of Gs-9973, a Selective and Orally Efficacious Inhibitor of Spleen Tyrosine Kinase. *J Med Chem*. 2014;57(9):3856-3873.
34. Walker AR, Byrd JC, Bhatnagar B, et al. Results of a Phase 1b/2 Study of Entospletinib (Gs-9973) Monotherapy and in Combination with Induction Chemotherapy in Newly Diagnosed Patients with Acute Myeloid Leukemia. *HemaSphere*. 2018;2(S1):11.
35. Salzer WL, Jones TL, Devidas M, et al. Decreased Induction Morbidity and Mortality Following Modification to Induction Therapy in Infants with Acute Lymphoblastic Leukemia Enrolled on Aall0631: A Report from the Children's Oncology Group. *Pediatr Blood Cancer*. 2015;62(3):414-418.
36. Maude SL, Tasian SK, Vincent T, et al. Targeting Jak1/2 and Mtor in Murine Xenograft Models of Ph-Like Acute Lymphoblastic Leukemia. *Blood*. 2012;120(17):3510-3518.
37. Maude SL, Dolai S, Delgado-Martin C, et al. Efficacy of Jak/Stat Pathway Inhibition in Murine Xenograft Models of Early T-Cell Precursor (Etp) Acute Lymphoblastic Leukemia. *Blood*. 2015;125(11):1759-1767.
38. Tasian SK, Teachey DT, Li Y, et al. Potent Efficacy of Combined Pi3k/Mtor and Jak or Abl Inhibition in Murine Xenograft Models of Ph-Like Acute Lymphoblastic Leukemia. *Blood*. 2017;129(2):177-187.
39. Tasian SK, Hurtz C, Wertheim GB, et al. High Incidence of Philadelphia Chromosome-Like Acute Lymphoblastic Leukemia in Older Adults with B-All. *Leukemia*. 2017;31(4):981-984.
40. Ding YY, Stern JW, Jubelirer TF, et al. Clinical Efficacy of Ruxolitinib and Chemotherapy in a Child with Philadelphia Chromosome-Like Acute Lymphoblastic Leukemia with Golga5-Jak2 Fusion and Induction Failure. *Haematologica*. 2018;103(9):e427-e431.
41. Irving J, Matheson E, Minto L, et al. Ras Pathway Mutations Are Prevalent in Relapsed Childhood Acute Lymphoblastic Leukemia and Confer Sensitivity to Mek Inhibition. *Blood*. 2014;124(23):3420-3430.

42. Walker AR, Bhatnagar B, Marcondes AMQ, et al. Interim Results of a Phase 1b/2 Study of Entospletinib (Gs-9973) Monotherapy and in Combination with Chemotherapy in Patients with Acute Myeloid Leukemia. *Blood*. 2016;128(22):2831-2831.
43. Walker AR, Byrd JC, Blum W, et al. Abstract 819: High Response Rates with Entospletinib in Patients with T(V;11q23.3);<Em>Kmt2a</Em> Rearranged Acute Myeloid Leukemia and Acute Lymphoblastic Leukemia. *Cancer Res*. 2018;78(13 Supplement):819.
44. Kohrer S, Havranek O, Seyfried F, et al. Pre-Bcr Signaling in Precursor B-Cell Acute Lymphoblastic Leukemia Regulates Pi3k/Akt, Foxo1 and Myc, and Can Be Targeted by Syk Inhibition. *Leukemia*. 2016;30(6):1246-1254.
45. van der Veer A, van der Velden VHJ, Willemse ME, et al. Interference with Pre-B-Cell Receptor Signaling Offers a Therapeutic Option for Tcf3-Rearranged Childhood Acute Lymphoblastic Leukemia. *Blood Cancer J*. 2014;4:e181.
46. Hurtz C, Tasian SK, Wertheim GB, et al. Redundant Jak, Src and Pi3 Kinase Signaling Pathways Regulate Cell Survival in Human Ph-Like All Cell Lines and Primary Cells. *Blood*. 2017;130(Suppl 1):717.
47. Hurtz C, Wertheim GB, Loftus JP, et al. Oncogene-Independent Adaptation of Pre-B Cell Receptor Signaling Confers Drug Resistance and Signaling Plasticity in Ph-Like All. *Blood*. 2019;134(Suppl 1):747.
48. Matheson EC, Thomas H, Case M, et al. Glucocorticoids and Selumetinib Are Highly Synergistic in Ras Pathway Mutated Childhood Acute Lymphoblastic Leukemia through Upregulation of Bim. *Haematologica*. 2019;104(9):1804-1811.
49. Agraz-Doblas A, Bueno C, Bashford-Rogers R, et al. Unraveling the Cellular Origin and Clinical Prognostic Markers of Infant B-Cell Acute Lymphoblastic Leukemia Using Genome-Wide Analysis. *Haematologica*. 2019;104(6):1176-1188.
50. Marschalek R. Another Piece of the Puzzle Added to Understand T(4;11) Leukemia Better. *Haematologica*. 2019;104(6):1098-1100.
51. Bueno C, Calero-Nieto FJ, Wang X, et al. Enhanced Hemato-Endothelial Specification During Human Embryonic Differentiation through Developmental Cooperation between Af4-Mll and Mll-Af4 Fusions. *Haematologica*. 2019;104(6):1189-1201.
52. Brown PA, Kairalla J, Wang C, et al. Addition of Flt3 Inhibitor Lestaurtinib to Post- Induction Chemotherapy Does Not Improve Outcomes in Mll-Rearranged Infant Acute Lymphoblastic Leukemia (All): Aall0631, a Children's Oncology Group Study. *Pediatr Blood Cancer*. 2016;63(S3):26233.
53. Levis M, Brown P, Smith BD, et al. Plasma Inhibitory Activity (Pia): A Pharmacodynamic Assay Reveals Insights into the Basis for Cytotoxic Response to Flt3 Inhibitors. *Blood*. 2006;108(10):3477-3483.
54. Cooper TM, Cassar J, Eckroth E, et al. A Phase I Study of Quizartinib Combined with Chemotherapy in Relapsed Childhood Leukemia: A Therapeutic Advances in Childhood Leukemia & Lymphoma (Tacl) Study. *Clin Cancer Res*. 2016;22(16):4014-4022.

55. Bernt KM, Zhu N, Sinha AU, et al. MII-Rearranged Leukemia Is Dependent on Aberrant H3k79 Methylation by Dot1l. *Cancer Cell*. 2011;20(1):66-78.
56. Daigle SR, Olhava EJ, Therkelsen CA, et al. Selective Killing of Mixed Lineage Leukemia Cells by a Potent Small-Molecule Dot1l Inhibitor. *Cancer Cell*. 2011;20(1):53-65.
57. Shukla N, Wetmore C, O'Brien MM, et al. Final Report of Phase 1 Study of the Dot1l Inhibitor, Pinometostat (Epz-5676), in Children with Relapsed or Refractory MII-R Acute Leukemia. *Blood*. 2016;128(22):2780-2780.
58. von Stackelberg A, Locatelli F, Zugmaier G, et al. Phase I/Phase II Study of Blinatumomab in Pediatric Patients with Relapsed/Refractory Acute Lymphoblastic Leukemia. *J Clin Oncol*. 2016;34(36):4381-4389.
59. Driessen EM, van Roon EH, Spijkers-Hagelstein JA, et al. Frequencies and Prognostic Impact of Ras Mutations in MII-Rearranged Acute Lymphoblastic Leukemia in Infants. *Haematologica*. 2013;98(6):937-944.
60. Prella C, Bursen A, Dingermann T, et al. Secondary Mutations in T(4;11) Leukemia Patients. *Leukemia*. 2013;27(6):1425-1427.
61. Kerstjens M, Driessen EM, Willekes M, et al. Mek Inhibition Is a Promising Therapeutic Strategy for MII-Rearranged Infant Acute Lymphoblastic Leukemia Patients Carrying Ras Mutations. *Oncotarget*. 2017;8(9):14835-14846.
62. Cremer A, Ellegast JM, Alexe G, et al. Resistance Mechanisms to Syk Inhibition in Acute Myeloid Leukemia. *Cancer Discov*. 2020;10(2):214-231.

## TABLES

**Table 1. Molecular and cytogenetic characteristics of ALL PDX models.**

ALL PDX model	COG USI	<i>KMT2A</i> status	Translocation	Disease status	Other genetic alterations
ALL185GD	PAVVRD	wild-type	<i>P2RY8-CRLF2</i> , <i>PAX5-AUTS2</i>	<i>de novo</i>	<i>JAK2</i> mut, <i>CDKN2A/B</i> del
ALL83GD	PAUFHC	wild-type	<i>P2RY8-CRLF2</i> , <i>PAX5-C20orf112</i>	<i>de novo</i>	<i>JAK2</i> del, <i>CDKN2A/B</i> del, <i>RTEL</i> del
ALL132GD	PAUXSA	wild-type	t(1;19) (q23;p13) with <i>TCF3-PBX1</i>	<i>de novo</i>	<i>KRAS</i> mut, <i>WHSC1</i> mut, gain <i>CCND3</i> , <i>MYB</i> , <i>ESR1</i>
ALL150MD	PAVEDG	<i>KMT2A-AFF1</i>	t(4;11) (q21;q23)	<i>de novo</i>	<i>KRAS</i> mut
ALL142MD	PAVBRV	<i>KMT2A-AFF1</i>	t(4;11) (q21;q23)	<i>de novo</i>	<i>NRAS</i> mut
ALL142MR	PAVBRV	<i>KMT2A-AFF1</i>	t(4;11) (q21;q23)	relapse	<i>NRAS</i> mut, <i>IKZF1</i> del, cnLOH of chr22
ALL3113MR	n/a	<i>KMT2A-AFF1</i>	t(4;11) (q21;q23)	<i>de novo</i>	<i>JAK2</i> mut, <i>p53</i> 17p del, <i>IKZF1</i> 7p del
ALL3103MR	n/a	<i>KMT2A-MLLT3</i>	t(9;11) (p21;q23)	relapse	none identified
ALL135MD	PAUYJT	<i>KMT2A-MLLT1</i>	t(11;19) (q23;p13.3)	<i>de novo</i>	none identified
ALL135MR	PAUYJT	<i>KMT2A-MLLT1</i>	t(11;19) (q23;p13.3)	relapse	none identified
ALL26MD	PASHFM	<i>KMT2A-MLLT1</i>	t(11;19) (q23;p13.3)	<i>de novo</i>	none identified
ALL26MR	PASHFM	<i>KMT2A-MLLT1</i>	t(11;19) (q23;p13.3)	relapse	partial 10q del, including <i>PTEN</i>

COG USI = Children's Oncology Group unique specific identifier, cnLOH = copy-neutral loss of heterozygosity, del = deletion, mut = mutation, n/a = not available.

## FIGURE LEGENDS

**Figure 1. Constitutive SYK signaling occurs in infant ALL.** Simple Western analysis of splenic lysates from human ALL PDX models demonstrated high basal phosphorylated SYK (pSYK) levels in the majority of infant non-*KMT2A*-rearranged (R) (light blue) and *KMT2A*-R (dark blue) ALL specimens. pSYK levels were relatively lower in most childhood non-*KMT2A*-R ALL specimens (red) and absent in splenic tissue from non-leukemia-injected NSG mice (grey). Total SYK levels were similar across all models. ALL PDX model names are specified above corresponding Simple Western data.

## **Figure 2. Activity and dose optimization of entospletinib monotherapy in *KMT2A*-R ALL.**

**(A)** Viably cryopreserved harvested human *KMT2A*-R ALL cells from murine PDX spleens (model ALL3103 with *KMT2A-MLL3* fusion) demonstrated dose-dependent inhibition of colony formation *in vitro* in methylcellulose colony assays after ENTO treatment for 14 days. Samples were plated in triplicate in methylcellulose-based medium and grown in 10% leukocyte-conditioned medium with 25% FBS and 2% BSA. Data are displayed as mean  $\pm$  SEM. **(B)** ALL3103 PDX mice were treated with vehicle (control) or ENTO chow at the specified concentrations for 4 weeks. Human CD45<sup>+</sup> CD19<sup>+</sup> ALL flow cytometric analysis of murine blood at weekly time points and **(C)** spleens at study endpoint demonstrated significant inhibition of ALL proliferation with ENTO treatment (mean  $\pm$  SEM). No difference in ALL burden was observed in 0.03% versus 0.07% ENTO-treated animals. **(D)** Terminal blood was collected from animals after 4 weeks of continuous ENTO chow consumption and evaluated for entospletinib levels. Data from individual animals are plotted as median interquartile range. ns = not significant by t-test. **(E)** Terminal spleens from individual mice were harvested, viably cryopreserved, lysed, and evaluated for levels of pSYK, SYK, cMYC, pERK and  $\beta$ -actin by Simple Western. \* $p < 0.05$ , \*\* $p < 0.01$ , \*\*\*\* $p < 0.0001$  as compared to control chow-fed mice by ANOVA with Tukey's post-test.

**Figure 3. *In vitro* activity of entospletinib in *KMT2A-R* ALL.** Viably cryopreserved *KMT2A-R* ALL PDX cells were exposed *in vitro* to 0.1% DMSO (vehicle control) or increasing concentrations of entospletinib (200 nM, 500 nM, 1  $\mu$ M) for 2 hours, then lysed and analyzed by Simple Western. Additional untreated (baseline) cells were lysed immediately following sample thaw. **(A)** Dose-dependent inhibition of the specified phosphoproteins was observed with ENTO in the ALL135MR PDX model (*KMT2A-MLLT1*, RAS wild-type), while **(B)** no treatment effect was seen in the 142MR PDX model (*KMT2A-AFF1*, *NRAS*-mutant).

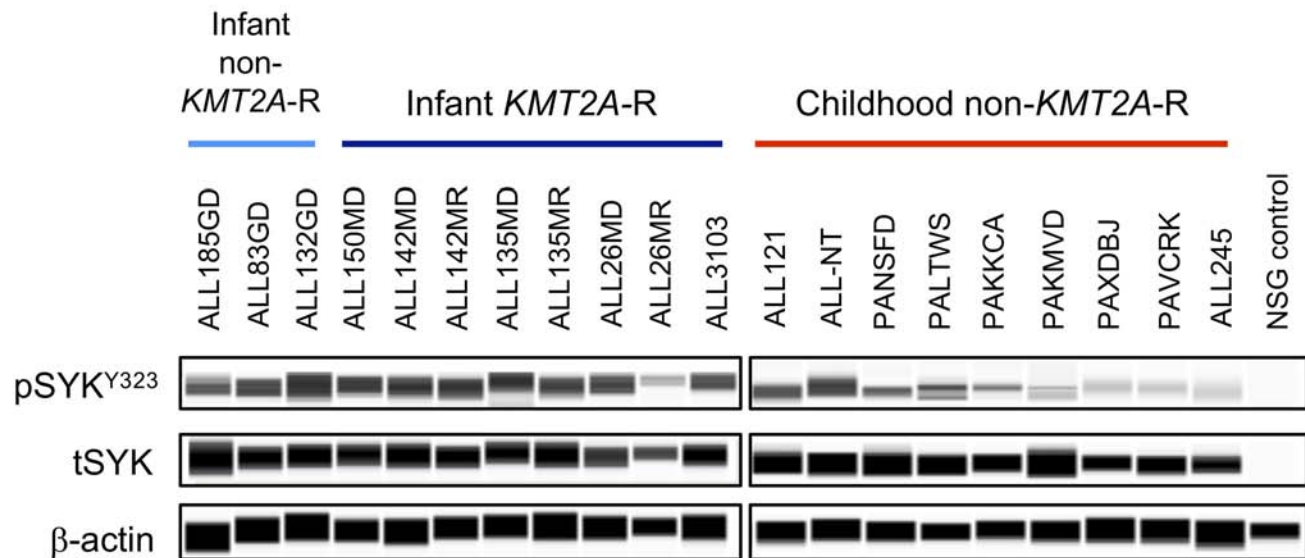
**Figure 4. *HOXA9* and *MEIS1* expression signatures of *KMT2A-R* and non-*KMT2A-R* ALL PDX specimens.** **(A)** Splenic PDX samples were analyzed for expression of mRNA for *HOXA9* and *MEIS1* by NanoString, with human bone marrow mononuclear cells (BMMC) and KG-1 cell line as negative and positive controls, respectively. Increased *MEIS1* and/or *HOXA9* expression was seen in *KMT2A-R* ALL PDX models versus non-*KMT2A-R* (WT) models and generally clustered by genetic subtype. **(B)** Total and phosphorylated signal transduction proteins from murine splenic lysates were evaluated using Simple Western. Basal kinase signaling activation differed among *KMT2A-R* and non-*KMT2A-R* ALL samples and stratified by genetic subgroup (*KMT2A-AFF1*, *KMT2A-MLLT1*, *KMT2A-MLLT3*, and non-*KMT2A-R*).  $\beta$ -actin was used as a protein loading control.

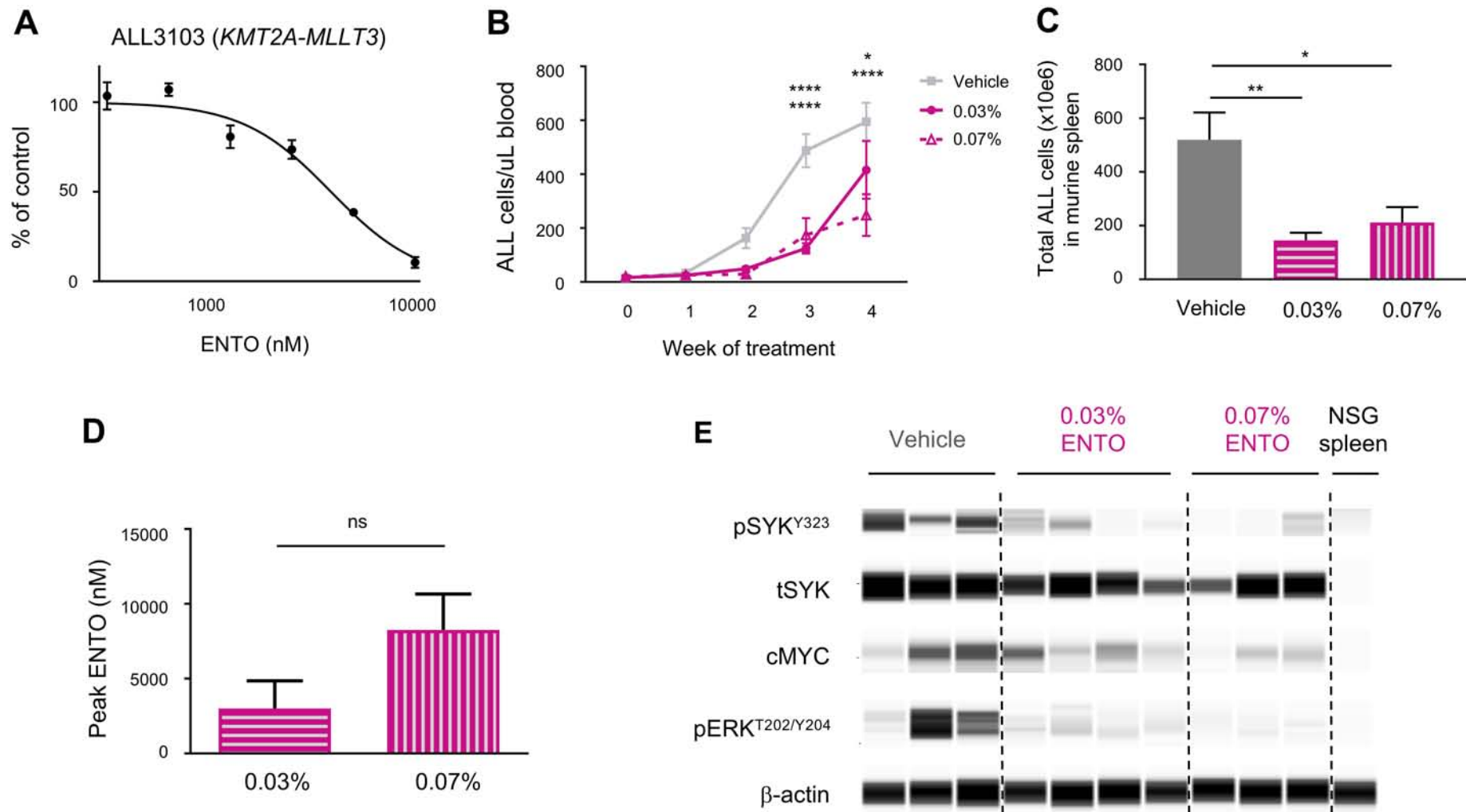
**Figure 5. Entospletinib potently inhibits *in vivo* ALL proliferation with enhanced efficacy in combination with chemotherapy.** Animals engrafted with *KMT2A-R* (ALL3103, ALL135MR, ALL142MR, ALL150MD, ALL3113) or non-*KMT2A-R* (ALL132GD, ALL185GD, ALL83GD) ALL were treated with control chow, 0.05% ENTO chow, 0.1 mg/kg vincristine (VCR) IP weekly, or both ENTO and VCR. Human CD45<sup>+</sup>CD19<sup>+</sup> ALL cells were quantified by flow cytometry in end-of-study murine spleens and peripheral blood. **(A)** Combined ENTO+VCR significantly inhibited leukemia proliferation with enhanced activity compared to ENTO and/or VCR monotherapies in

*KMT2A-R* PDX models without RAS mutations. **(B)** Conversely, potent VCR effects were observed in *KMT2A-R* ALL PDX models with *NRAS* or *KRAS* mutations without additional activity of combination treatment. **(C)** A *KMT2A-R* RAS wild-type ALL PDX model was sensitive to ENTO and not to VCR. **(D)** No treatment effects of ENTO or VCR were observed in a non-*KMT2A-R* *KRAS*-mutant ALL PDX model, while single-agent activity of VCR and/or ENTO and enhanced effects of combination treatment were detected in **(E)** non-*KMT2A-R* RAS wild-type PDX control models with other ALL-associated translocations. Data were analyzed by one-way ANOVA with Tukey's post-test for multiple comparisons. \* $p < 0.05$ , \*\* $p < 0.01$ , \*\*\*  $p < 0.001$ , \*\*\*\*  $p < 0.0001$ .

**Figure 6. Superior preclinical activity of entospletinib and selumetinib in *KMT2A-R* ALL PDX models.** **(A)** PDX models 142MR (*KMT2A-AFF1*, *NRAS*-mutant) and **(B)** ALL3113 (*KMT2A-AFF1*, RAS wild-type) were treated with vehicle control chow, 0.05% ENTO chow, 100 mg/kg selumetinib (SEL) via oral gavage twice daily 5 days/week, or both ENTO and SEL for 2 or 4 weeks. Human CD45+ CD19+ ALL cells were quantified by flow cytometry in peripheral blood and end-study murine spleens. Enhanced anti-leukemia efficacy was observed in both models with combined ENTO and SEL treatment versus ENTO or SEL alone, as measured by one-way ANOVA with post Tukey's post-test for multiple comparisons. \* $p < 0.05$ , \*\* $p < 0.01$ , \*\*\*\*  $p < 0.0001$ . **(C)** *Ex vivo* phosphoflow cytometry analysis of gated human CD19+ CD45+ ALL cells in end-study murine spleens after 2 weeks (ALL142MR) or 4 weeks (ALL3113) of ENTO and/or SEL treatment demonstrate inhibition of pSYK, pERK, and/or pS6 versus vehicle control (grey). ns = not significant, \* $p < 0.05$ , \*\* $p < 0.01$  by one-way ANOVA with post Tukey's post-test for multiple comparisons.

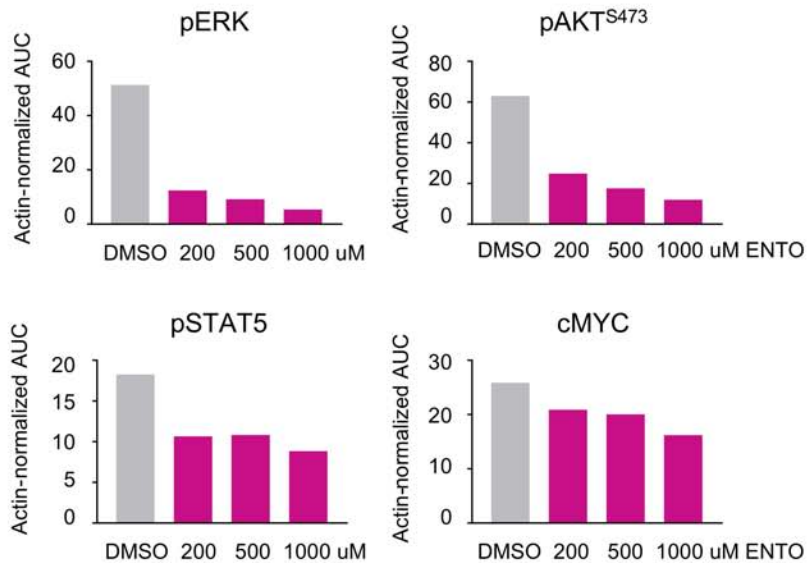
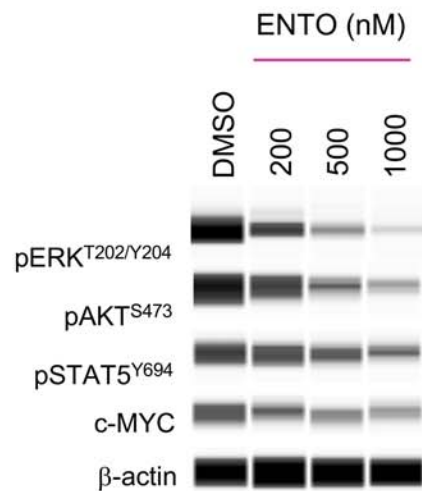
# Figure 1



**Figure 2**

# Figure 3

## A ALL135MR (*KMT2A-MLLT1*)



## B ALL142MR (*KMT2A-AFF1*, RAS-mutant)

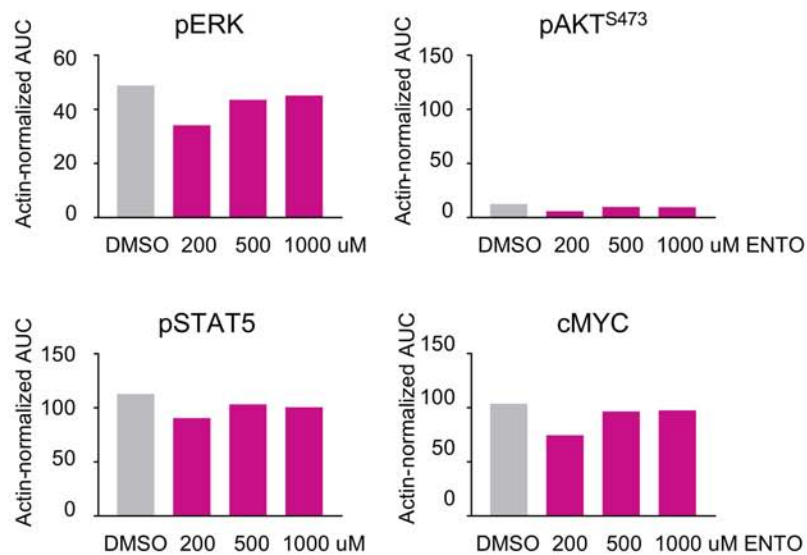
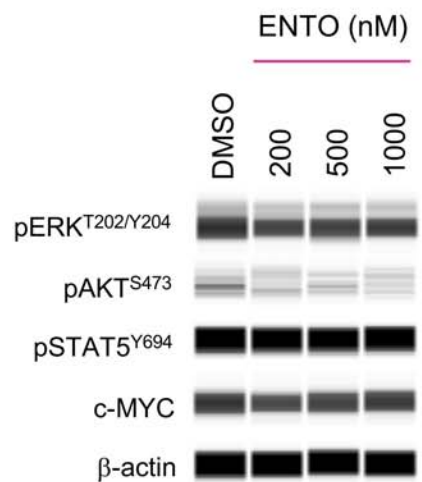
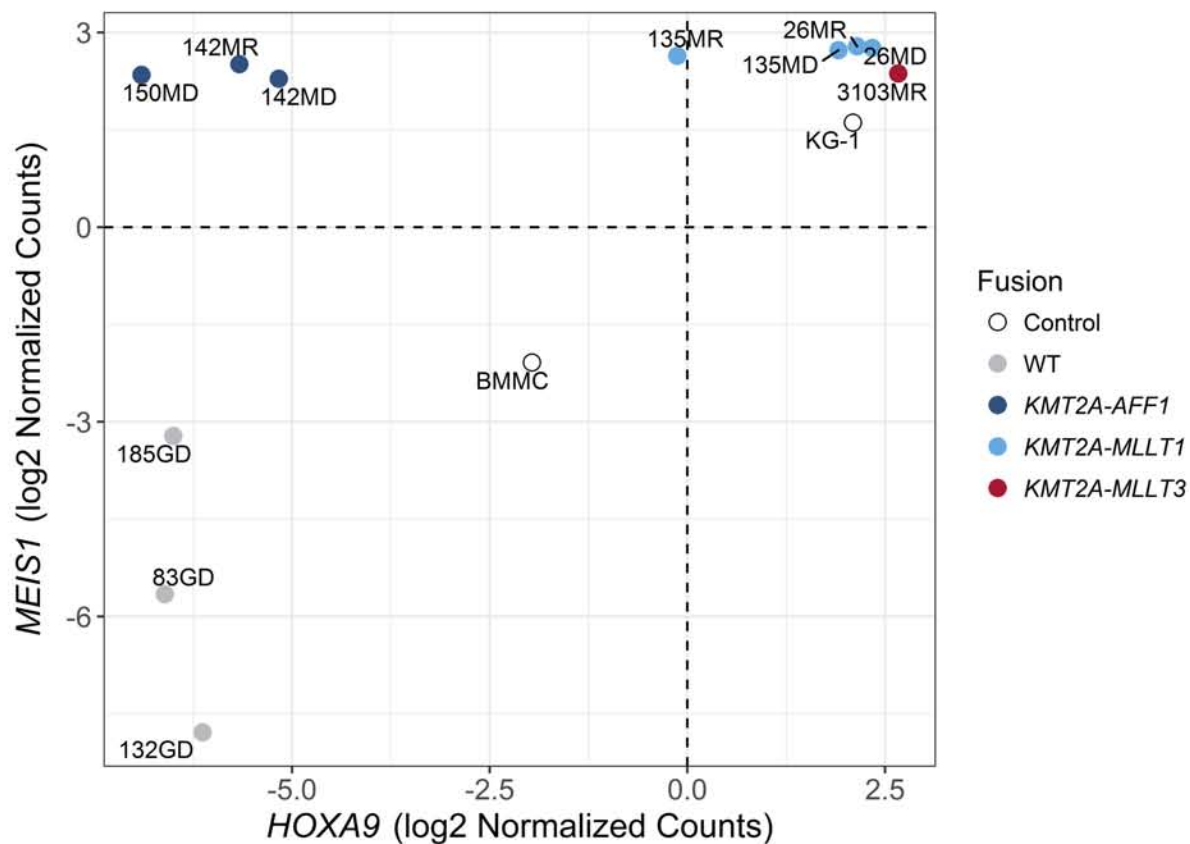


**Figure 4**

**A**



**B**

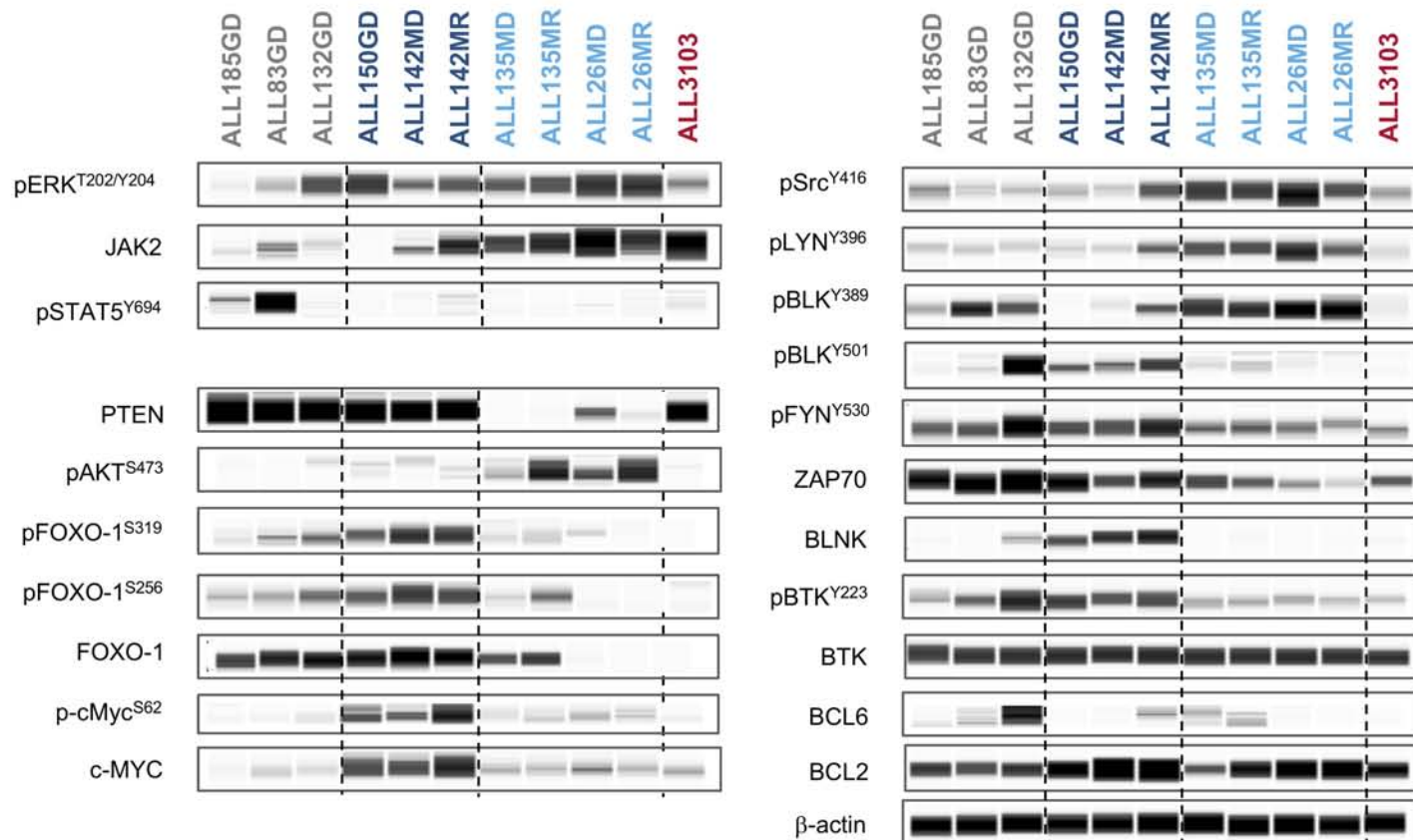
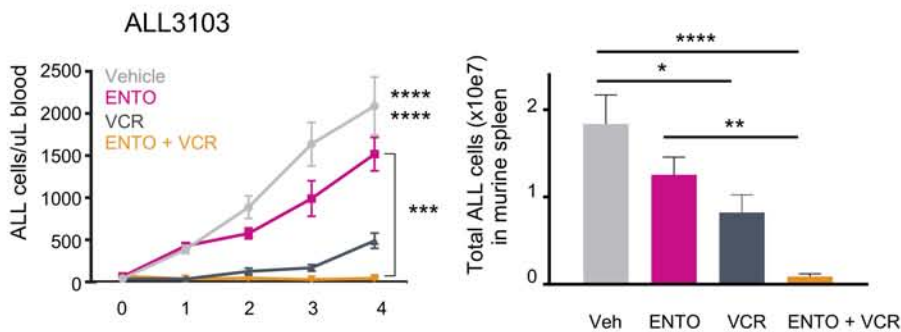
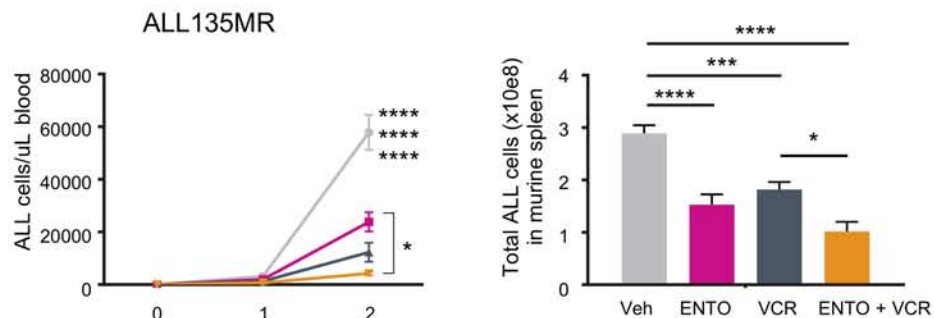


# Figure 5

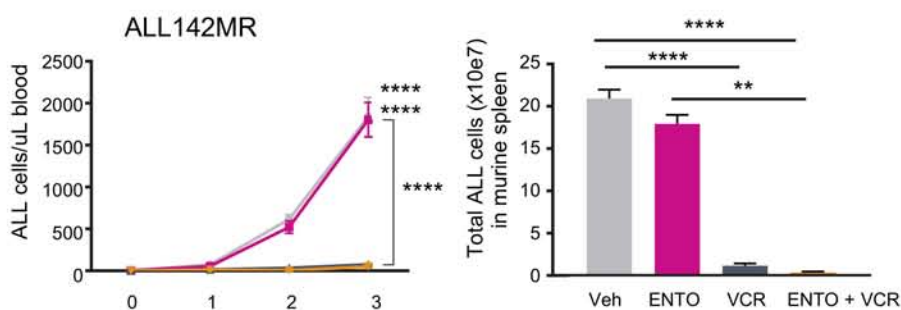
## A *KMT2A-MLLT3*, RAS wild-type



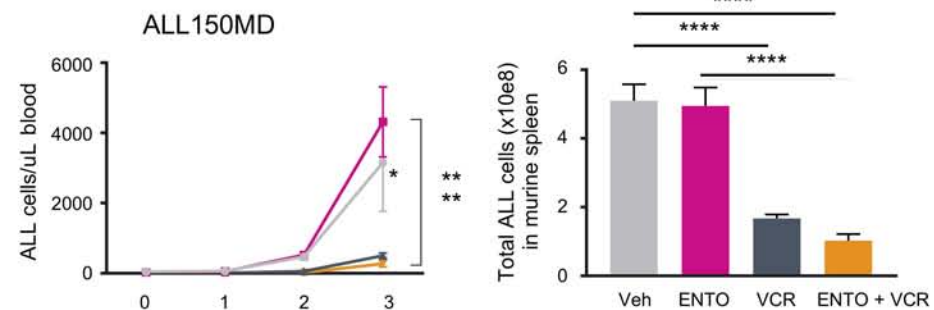
## *KMT2A-MLLT1*, RAS wild-type



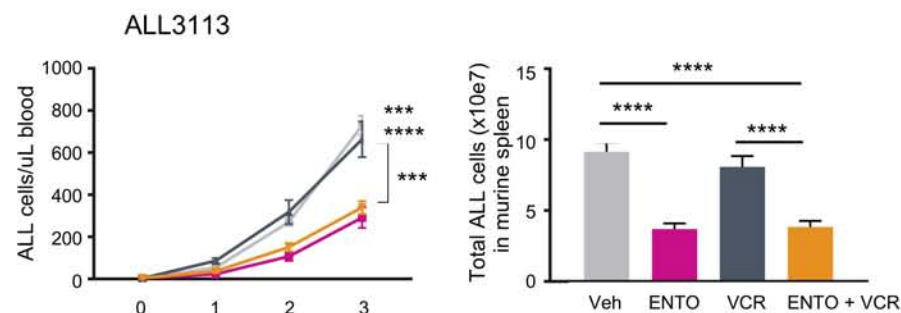
## B *KMT2A-AFF1*, RAS-mutant



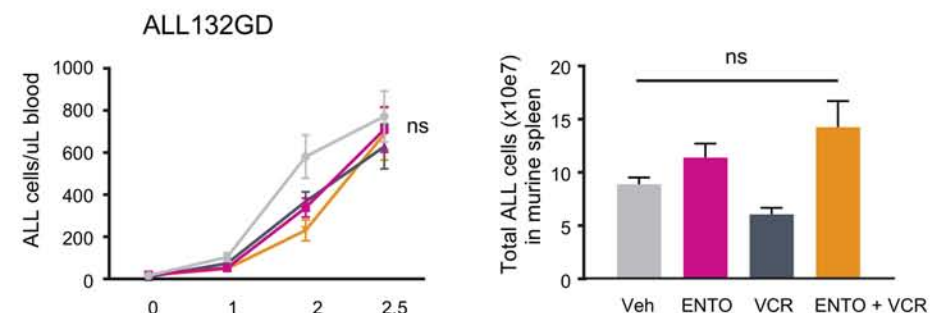
## *KMT2A-AFF1*, RAS-mutant



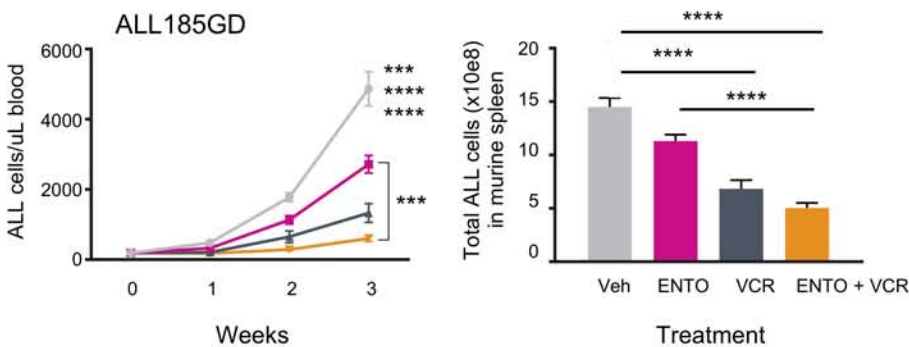
## C *KMT2A-AFF1*, RAS wild-type



## D non-*KMT2A-R*, RAS-mutant



## E Non-*KMT2A-R*, RAS wild-type



## Non-*KMT2A-R*, RAS wild-type

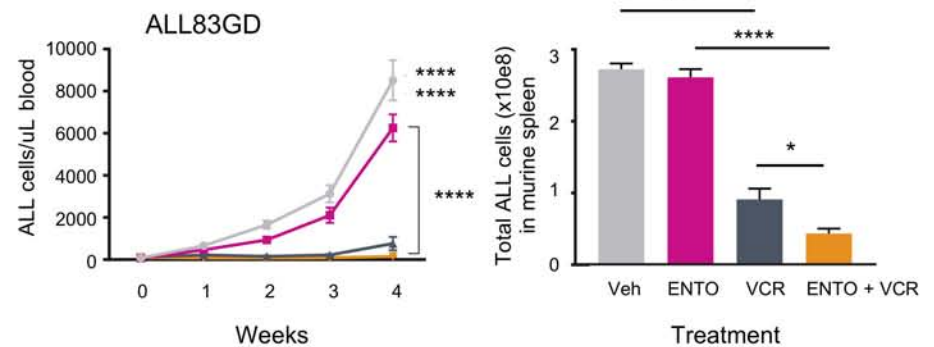
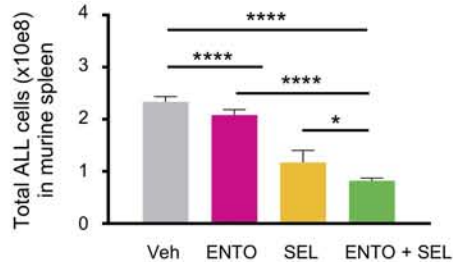
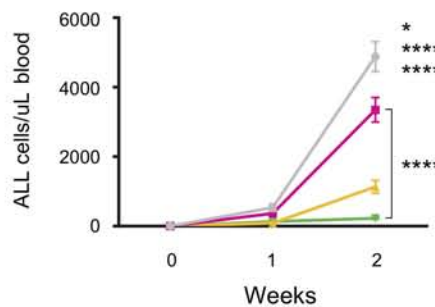


# Figure 6

**A**

*KMT2A-AFF1*, RAS-mutant

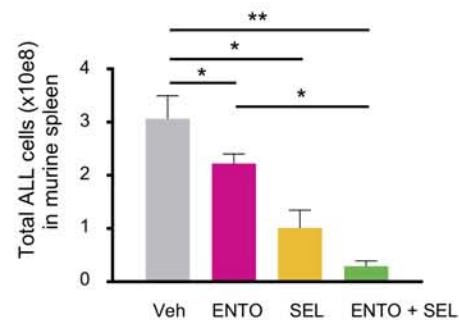
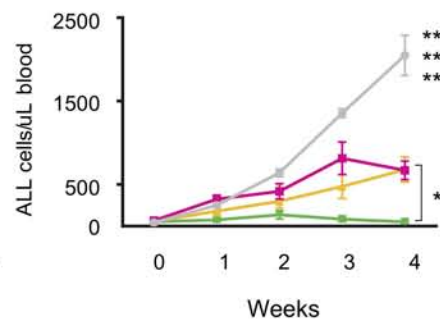
ALL142MR



**B**

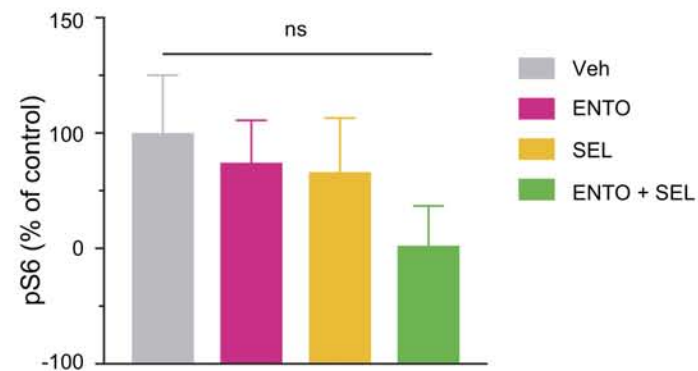
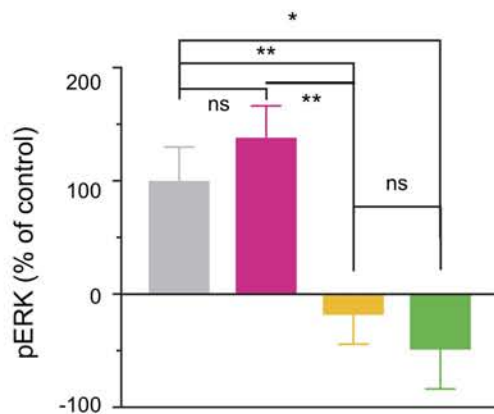
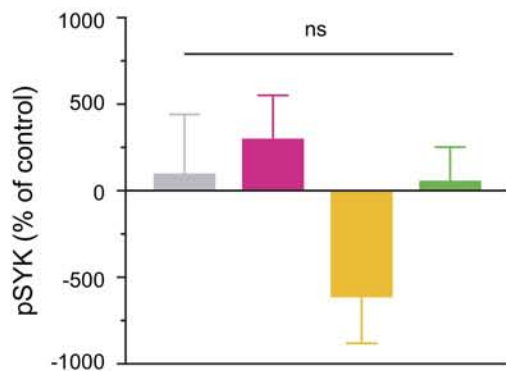
*KMT2A-AFF1*, RAS wild-type

ALL3113



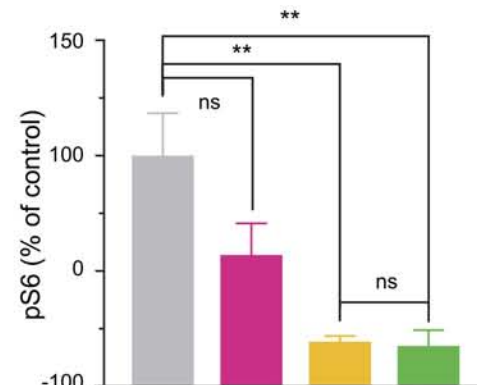
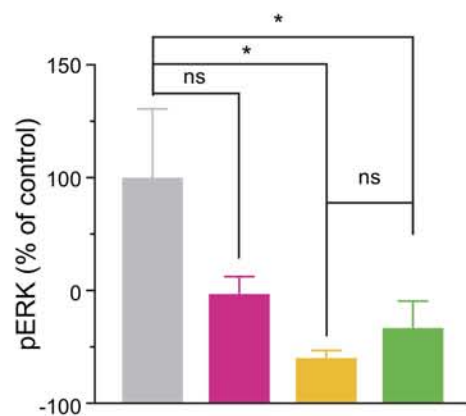
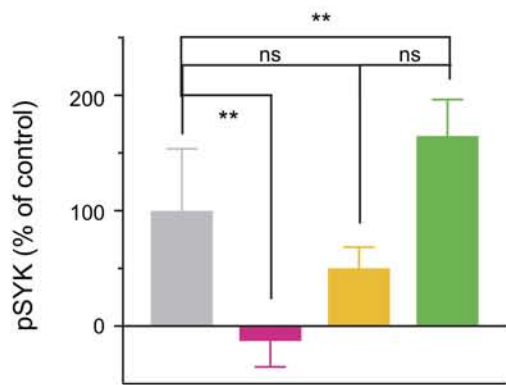
**C**

ALL142MR



**D**

ALL3113



## SUPPLEMENTAL DATA

### SUPPLEMENTAL METHODS

#### *Cell Titer Glo viability assays*

The human B-acute lymphoblastic leukemia (B-ALL) cell lines NALM-6 (non-*KMT2A*-rearranged) and HB11;19, KOPN-8, and HB11;19 (all *KMT2A*-rearranged) were obtained from the German Collection of Microorganisms and Cell Cultures GmbH (Deutsche Sammlung von Mikroorganismen und Zellkulturen; DSMZ), validated by short tandem repeat identity testing, and confirmed to be *Mycoplasma*-free. ALL cells were incubated *in vitro* with dimethyl sulfoxide or increasing concentrations of entospletinib (Gilead Sciences), fostamatinib (Selleckchem), dasatinib (LC Labs), selumetinib (LC Labs), and/or dexamethasone as indicated in Supplemental Figure 1 for 72 hours, then assessed for cell viability via Cell Titer Glo luminescent assays (Promega) according to manufacturer's instructions using an IVIS Spectrum bioluminescent imaging instrument and Living Image software (PerkinElmer) (1, 2). Data were analysed and displayed graphically in Prism (**Supplemental Figure 1**, **Supplemental Figure 4**, and **Supplemental Figure 5**).

#### *Phosphoflow cytometry*

Viably cryopreserved murine spleen cells from well-engrafted B-ALL PDX models were thawed, washed once in ice-cold serum-free Iscove's modified Dulbecco's medium (IMDM), treated *in vitro* with vehicle, entospletinib, fostamatinib, dasatinib, and/or selumetinib at 37 °C for 60 minutes and then fixed in 16% paraformaldehyde and permeabilized in 90% high-grade methanol as described (3) (**Supplemental Figure 2** and **Supplemental Figure 3**). Human B-ALL cell lines were also incubated *in vitro* with 100 nM, 500 nM, or 1000 nM entospletinib and/or selumetinib in IMDM at 37 °C for 60 minutes prior to fixation and permeabilization as described for phosphoflow cytometry analysis (4, 5) (**Supplemental Figure 6**). Harvested ALL cells from

end-study murine spleens from control or drug-treated PDX models were also analysed by phosphoflow cytometry via the above methodologies (**Figure 6**). ALL cell line and PDX cells were stained with CD45-APC and CD19- APC-eFluor780 (both from EBioscience) cell surface markers and with phosphorylated (p) ERK<sub>T202/Y204</sub>-PacBlue, and pS6<sub>S240/244</sub>-Ax594 or pSYK<sub>Y525/526</sub>-PacBlue (all from Cell Signaling Technologies) intracellular antibodies. Data were collected on a BD FACSVerse flow cytometer with data analysis in Cytobank and graphic display in Prism as described (6).

#### *In vitro colony formation assays*

Viably cryopreserved infant *KMT2A*-rearranged ALL cells harvested from a well-engrafted murine PDX model (ALL3103) were thawed in StemSpan™ SFEM II medium (Stemcell Technologies; Vancouver, BC, Canada) supplemented with recombinant human IL-3 10 ng/mL, granulocyte-macrophage colony-stimulating factor 10 ng/mL, stem cell factor 50 ng/mL (all from Peprotech; Rocky Hill, NJ), and penicillin/streptomycin and rested for 1 hour at 37 °C. ALL cells were subsequently plated in triplicate in 35 mm sterile plates (Cellstar) at 4x10<sup>4</sup> cells/well in cytokine- and antibiotic-containing methylcellulose medium with 25% FBS and 2% BSA and with dimethyl sulfoxide (DMSO; negative control) or increasing concentrations of ENTO. Colony growth was enumerated after 14 days and confirmed to be of lymphoid origin with data analysis and display in Prism (GraphPad; San Diego, CA).

#### *Immunoblotting studies*

Additional ALL PDX cells were thawed and rested for 1 hour at 37°C as above, then treated for 2 hours with 0.1% DMSO or 1 uM entospletinib prior to cell lysis (using Cell Signaling Technology [CST] lysis buffer with protease inhibitor cocktail [Roche Diagnostics] and phosphatase inhibitor sets 1 and 2 [EMD Millipore]) and subsequent evaluation of total and

phosphoprotein expression. Following 30 minutes on ice, cell lysates were cleared by centrifugation at 12,600 rpm for 10 minutes at 4°C. Lysates were analyzed by Simple Western using Peggy Sue™ and Sally Sue™ (ProteinSimple, San Jose, CA; subsequently termed Simple Western).

The following total and phosphorylated protein antibodies were used for Simple Western assays: pERK1/2<sub>T202/Y204</sub>, JAK2, pSTAT5<sub>Y694</sub>, PTEN, pAKT<sub>S473</sub>, pFOXO-1<sub>S256</sub>, pFOXO-1<sub>S319</sub>, FOXO-1, pSRC<sub>Y416</sub>, pLYN<sub>Y396</sub>, ZAP70, pBTK<sub>Y223</sub>, BTK, BCL6, BCL2, BLNK, β-actin (all from CST), p-cMYC<sub>S62</sub>, c-MYC, pFYN<sub>Y530</sub> (Abcam), pBLK<sub>Y389</sub>, pBLK<sub>Y501</sub> (ThermoFisher), pSYK<sub>Y323</sub> (EMD Millipore), and total SYK (Santa Cruz Biotechnology).

#### *In vivo testing of kinase inhibitors and chemotherapy in ALL PDX models*

Following treatment initiation with kinase inhibitors and/or chemotherapy, patient-derived xenograft (PDX) mice were followed by weekly quantitative flow cytometry (FC) analysis of human ALL in retro-orbital venous blood samples and at study endpoint in harvested murine tissues (6). PK analysis of murine blood samples was performed by Gilead Sciences as described (7). Spleen and bone marrow tissues from PD studies were analysed by Simple Western analysis as described below. FC data were captured on a FACSVerse flow cytometer (BD Biosciences) and analysed in Cytobank. Human ALL cell numbers in murine spleens and peripheral blood of vehicle- and drug-treated animals were evaluated for statistical significance by one-way ANOVA with Tukey's post-test for multiple comparisons and displayed graphically in Prism (**Figure 2, Figure 5, Figure 6, Supplemental Figure 7**). Pharmacokinetic-pharmacodynamic correlation analysis was performed in 'short term' AALL3103 PDX mice treated with entospletinib for 72 hours to assess potential dose-dependent inhibition of pSYK<sub>Y323</sub> and pERK<sub>T202/Y204</sub> (**Supplemental Figure 8**).

### *Gene expression analyses*

Gene expression data were analyzed using the NanoStringQCPro R package, version 1.14.10. After positive control normalization and background adjustment using the internal control probes included in the panel, data were log<sub>2</sub>-transformed and normalized using default housekeeping genes. Differential gene expression between *KMT2A-R* versus wild-type or between *KMT2A-MLLT1* versus *KMT2A-AFF1* samples were assessed and compared using the LIMMA R-package (8). Genes with 2-fold difference and p-value <0.05 were identified as significantly expressed (**Supplemental Figure 9**).

### *Immunohistochemistry studies*

Confirmatory immunohistochemical analysis of CD19+ human ALL in harvested murine tissues was performed for some studies. Formalin-fixed, paraffin-embedded ALL-engrafted murine spleen and femur tissues were sectioned (Leica, RM2255 microtome) at 5 µm thickness, placed on Super Frost Plus glass microscope slides (VWR, 48311-703), and baked at 60°C for 20 minutes. Sections were deparaffinized on the DISCOVERY Ultra (Roche Ventana) autostainer at 68°C for 12 minutes. Target epitope retrieval was then performed using heat induced epitope retrieval with Cell Conditioning Solution CC1 (Roche Ventana, 950-124) for 64 minutes at 95°C. The rabbit monoclonal primary anti-CD19 antibody (Abcam, ab134114) was diluted 1:800 in Da Vinci Green diluent (Biocare Medical, PD900M) and incubated for 40 minutes with no heat. A secondary DISCOVERY anti-rabbit-HQ (Roche Ventana, 760-4815) antibody was incubated at 37°C for 32 minutes. The tertiary detection step used DISCOVERY anti-HQ-HRP (Roche Ventana, 760-4820) for 32 minutes at 37°C. Signal visualization used DISCOVERY ChromoMap DAB kit (Roche Ventana, 750-159) at 37°C. Lastly, tissue samples were counterstained with Hematoxylin II (Roche Ventana, 790-2208) at room temperature for 4 minutes.

Upon completion of staining, slides were rinsed in deionized water and soap to remove the oil-based liquid cover slips and were dehydrated by 2 minute incubations in the following

sequence: 1) 70% ethanol 2) 80% ethanol 3) 90% ethanol 4) 100% ethanol 5) 100% ethanol 6) xylene 7) xylene. Slides were then cover-slipped using the Dako Coverslipper (Dako, CR100) with 24mm x 50mm cover glass (Dako, CS70430-2) and mounting media (Dako, CS703) (**Supplemental Figure 10**).

#### *Quantitative Morphometric Measurement of CD19 Staining*

Whole slide-scan images of IHC stained slides were imaged using the Aperio® AT2 (Leica Biosystems) at 40x magnification. Digital slide images were checked for scanning quality, annotated and exported to appropriate network folders within Leica Slidepath Digital Image Hub archive. Quantitative image analysis of CD19-stained tissues was performed on the whole slide-scan images using Visiopharm 2017.2 and the Tissue Find application. A subsequent application was implemented to detect the cells with positive CD19 expression. Positive expression quantification was categorized in three groups (low, medium, high) based on the level of signal intensity and used to calculate an H-score with the equation below (**Supplemental Figure 10**).

$$\%area = \frac{Low\ expression + medium\ expression + high\ expression}{entire\ tissue\ area} \times 100$$
$$H - score = \frac{Low\ expression \times 1 + medium\ expression \times 2 + high\ expression \times 3}{entire\ tissue\ area} \times 100$$

**SUPPLEMENTAL TABLE**

**Supplemental Table 1. Molecular and cytogenetic characteristics of non-infant ALL PDX models.**

<b>ALL PDX model</b>	<b>COG USI</b>	<b>Ph-like</b>	<b>Translocation</b>	<b>Disease status</b>	<b>Other genetic alterations</b>
<b>ALL121</b>	n/a	yes	<i>IGH-CRLF2</i>	relapse	<i>JAK2</i> R683G, <i>CDKN2A/B</i> del
<b>ALL-NT</b>	PATYEI	yes	<i>RCSD1-ABL1</i>	relapse	
<b>PHL3</b>	PANSFD	yes	<i>ETV6-ABL1</i>	<i>de novo</i>	
<b>NH362</b>	PALTWS	no	<i>IGH-CRLF2</i>	<i>de novo</i>	<i>FLT3</i> N609ins23aa
<b>NL432</b>	PAKKCA	yes	<i>EBF1-PDGFRB</i>	<i>de novo</i>	
<b>JL491</b>	PAKMVD	yes	none	<i>de novo</i>	<i>JAK1</i> S646F
n/a	PAXDBJ	yes	<i>GOLGA5-JAK2</i>	<i>de novo</i>	<i>CDKN2A/B</i> del, <i>IKZF1</i> del, <i>PAX5</i> del
n/a	PAVCRK	yes	<i>IGH-EPOR</i>	<i>de novo</i>	<i>CDKN2A/B</i> del, <i>IKZF1</i> del
<b>ALL245</b>	PAWTKG	yes	<i>IGH-CRLF2</i>	<i>de novo</i>	<i>JAK1</i> R629_I631delinsPL, <i>IKZF1</i> del

COG USI = Children's Oncology Group unique specific identifier, del = deletion, mut = mutation, n/a = not available, Ph-like = positive kinase expression signature by low-density microarray testing. Some ALL PDX models were previously published in Maude *et al* Blood 2012, Iacobucci *et al* Cancer Cell 2016, Tasian *et al* Blood 2017, and Ding *et al* Haematologica 2018.

## SUPPLEMENTAL FIGURES

**Supplemental Figure 1. Viability assays of SYK inhibitor-treated *KMT2A*-rearranged ALL cell lines.** Non-*KMT2A*-rearranged (NALM-6) and *KMT2A*-rearranged (HB11;19, KOPN-8, SEM) B-ALL cell lines were treated *in vitro* with kinase inhibitors entospletinib, fostamatinib, or dasatinib at the indicated concentrations for 72 hours, and cell viability was assessed via Cell Titer Glo assays. Half-maximal inhibitory concentrations (IC50) for each inhibitor and cell line are tabulated and displayed. *KMT2A*-rearranged cell lines show similar sensitivity profiles to the more selective SYK inhibitors entospletinib and fostamatinib (with the exception of KOPN-8), but are relatively resistant to the multi-kinase inhibitor dasatinib.

**Supplemental Figure 2. Basal signaling activation in non-*KMT2A*-rearranged and *KMT2A*-rearranged ALL PDX models.** Non-*KMT2A*-rearranged (ALL185GD, ALL83GD, ALL132GD; grey), *KMT2A-AFF1* (ALL150MD, ALL142MD, ALL142MR, ALL3113; dark blue), *KMT2A-MLLT3* (ALL3103MR; red), and *KMT2A-MLLT1* (ALL26MD, ALL26MR, ALL135MD, ALL135MR; light blue) B-ALL PDX cells harvested from viably-cryopreserved murine spleens were thawed and incubated *in vitro* in serum-free medium for 1 hour at 37 °C prior to fixation and permeabilization, cell surface and intracellular antibody staining, and phosphoflow cytometric analysis. Fluorescence-minus-one (FMO) controls were used for each fluorophore-conjugated phosphoprotein antibody to set negative (FMO-) and positive (FMO+) gates. Basal levels of phosphorylated (p) SYK<sub>Y525/526</sub>, pERK1/2<sub>T202/Y204</sub>, and pS6<sub>S240/244</sub> were quantified by phosphoflow cytometry and displayed as percentages of CD45+ CD19+ human ALL cells in FMO+ gates as previously described (6). ALL3113 (dotted dark blue) was created from an adult *KMT2A*-rearranged specimen. All other PDX models were established from *de novo* or relapsed infant ALL specimens from the Children's Oncology Group AALL0631 phase 3 clinical trial or institutional leukemia biorepositories.

**Supplemental Figure 3. Phosphoflow cytometry analysis of kinase inhibitor-treated ALL PDX cells.** Non-*KMT2A*-rearranged (ALL185GD, ALL83GD, ALL132GD) and *KMT2A*-rearranged (all others) B-ALL PDX cells were harvested from murine spleens and treated *in vitro* with 1  $\mu$ M entospletinib, fostamatinib, or dasatinib in serum-free medium for 1 hour at 37 °C prior to fixation and permeabilization, cell surface and intracellular antibody staining, and phosphoflow cytometric analysis as in Supplemental Figure 2. The phosphatase inhibitor pervanadate at 125  $\mu$ M final concentration was used as a positive signaling control (not shown). Phosphoprotein levels were normalized to basal conditions (DMSO-treated controls) in each model, and percent signaling inhibition was calculated for each drug treatment as described (6). Most PDX models demonstrated inhibition of pSYK<sub>Y525/526</sub>, pERK1/2<sub>T202/Y204</sub>, and/or pS6<sub>S240/244</sub> with *in vitro* kinase inhibitor treatment. Similar effects of the selective SYK inhibitors entospletinib and fostamatinib were observed in most models.

**Supplemental Figure 4. *In vitro* and *in vivo* evaluation of entospletinib and dexamethasone in ALL PDX models.** (A) Non-*KMT2A*-rearranged (NALM-6) and *KMT2A*-rearranged (HB11;19, KOPN-8, SEM) B-ALL cell lines were treated *in vitro* with dexamethasone without (left panel) or with 1  $\mu$ M entospletinib (right panel) at the indicated concentrations for 72 hours, and cell viability was assessed via Cell Titer Glo assays. KOPN-8 cells were relatively more glucocorticoid-resistant, but appeared to be resensitized to dexamethasone with concomitant entospletinib exposure. (B) *KMT2A*-rearranged ALL3113MR and (C) non-*KMT2A*-rearranged ALL83GD PDX models were treated with control chow (vehicle [veh]), entospletinib (ento) 0.05% chow continuously provided, dexamethasone (dex) 1 mg/kg intraperitoneally 5 days/week, or both ento and dex for 4 weeks. Human CD45<sup>+</sup> CD19<sup>+</sup> ALL flow cytometric analysis of murine blood at weekly time points (left panels) and spleens at study endpoint (right panels) demonstrated significant inhibition of ALL proliferation with dex treatment (mean  $\pm$  SEM). No additional reduction of splenic leukemia burden was observed in either PDX model with combination ento/dex

treatment. Data were analysed in Prism via ANOVA with Dunnett's (blood data) or Tukey's (spleen data) post-test for multiple comparisons. ns = not significant, \*  $p < 0.05$ , \*\*  $p < 0.01$ , \*\*\*  $p < 0.001$ , \*\*\*\*  $p < 0.0001$ .

**Supplemental Figure 5. Viability assays of kinase inhibitor-treated *KMT2A*-rearranged ALL cell lines.** Non-*KMT2A*-rearranged (NALM-6) and *KMT2A*-rearranged (HB11;19, KOPN-8, SEM) B-ALL cell lines were treated *in vitro* with (A) the SYK inhibitor entospletinib, (B) the MEK inhibitor selumetinib, or (C) and (D) both inhibitors at the indicated concentrations for 72 hours, and cell viability was assessed via Cell Titer Glo assays. RAS-mutant cell lines NALM-6 and KOPN-8 were particularly sensitive to selumetinib.

**Supplemental Figure 6. Phosphoflow cytometry analysis of kinase inhibitor-treated *KMT2A*-rearranged ALL cell lines.** Non-*KMT2A*-rearranged (NALM-6) and *KMT2A*-rearranged (HB11;19, KOPN-8, SEM) B-ALL cell lines were treated *in vitro* with the SYK inhibitor entospletinib and/or the MEK inhibitor selumetinib at the indicated concentrations in serum-free medium for 1 hour prior to fixation and permeabilization, cell surface and intracellular antibody staining, and phosphoflow cytometric analysis as in Supplemental Figure 2. Pervanadate 125  $\mu\text{M}$  final concentration was used as a positive signaling control (not shown).

**Supplemental Figure 7. *In vivo* activity of entospletinib monotherapy in Ph-like ALL.** NH011 PDX mice were treated with vehicle (veh) or ento chow at the specified concentrations (0.03%, 0.07%) for 3 weeks with the same methods used for the ALL3103 model data shown in Figure 2. Human CD45+ CD19+ ALL flow cytometric analysis of murine blood at weekly time points (left panel) and spleens at study endpoint (right panel) demonstrated significant inhibition of ALL proliferation with ENTO treatment (mean  $\pm$  SEM). No difference in ALL burden was observed in 0.03% versus 0.07% ENTO-treated animals. Data were analysed in Prism via ANOVA with

Tukey's post-test for multiple comparisons. ns = not significant, \*  $p < 0.05$ , \*\*  $p < 0.01$ , \*\*\*  $p < 0.001$ , \*\*\*\*  $p < 0.0001$ .

**Supplemental Figure 8. Pharmacokinetic and pharmacodynamic correlation in an entospletinib-treated ALL PDX model.** Individual mice from the ALL3103 (*KMT2A-MLLT3*) PDX model treated with ENTO for 72 hours demonstrated a correlation between higher ENTO concentration and lower pSYK Y323 expression (Pearson correlation coefficient  $r = -0.627$ ;  $p = 0.01$ ) and pERK 1/2 expression (Pearson correlation coefficient  $r = -0.303$ ;  $p = 0.31$ ). Terminal spleens were harvested, viably cryopreserved, lysed, and evaluated for levels of pSYK, pERK and  $\beta$ -actin by Simple Western; area under the curve (AUC) values were normalized to  $\beta$ -actin loading control. Terminal blood was collected and evaluated for entospletinib levels.

**Supplemental Figure 9. Immunohistochemical analysis of murine tissues after *in vivo* entospletinib treatment.** CD19 staining via immunohistochemistry (IHC) was performed in harvested spleens and bone marrow of mice engrafted with ALL3103 (*KMT2A-MLLT3*) cells and treated for 4 weeks with vehicle control (saline), 0.07% ENTO chow, 0.25 mg/kg vincristine (VCR), or ENTO and VCR in combination. Percentage represents median of %CD19+ area stained per treatment group. CD19 staining in naïve (non-leukemia-engrafted) mice is displayed in the graph, but not included in statistical analysis. Data are represented as median with interquartile range. \* $p < 0.05$ , \*\* $p < 0.01$ , \*\*\*\*  $p < 0.0001$  by one-way ANOVA with post-hoc Tukey's test for multiple comparisons.

**Supplemental Figure 10. Differential gene expression between *KMT2A*-R and non-*KMT2A*-R PDX models.** Transcriptomic differences between 3 non-*KMT2A*-rearranged (ALL83GD, ALL132GD, ALL185GD) and 8 *KMT2A*-rearranged (others) ALL PDX model samples were evaluated using NanoString. **(A)** Forty-seven upregulated genes and 23 downregulated genes

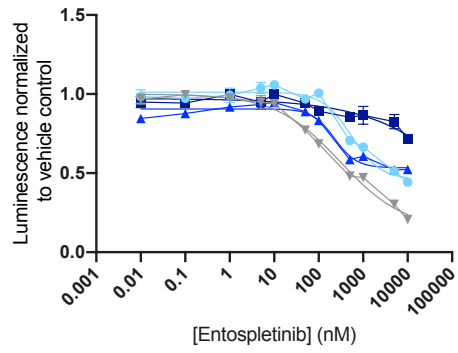
were identified in *KMT2A*-R (left) samples in comparison to non-*KMT2A*-R (right) ALL samples, demonstrating clear separation of these genetic subtypes. **(B)** Further analysis of *KMT2A*-R ALL samples demonstrated 116 significantly differential expressed genes in samples with *KMT2A*-*MLL1* (n=2) versus *KMT2A*-*AFF1* (n=2) rearrangements, including genes involved in DNA repair, cell cycle/apoptosis, and MAPK, PI3K, and RAS signaling pathways.

## SUPPLEMENTAL REFERENCES

1. Gill S, Tasian SK, Ruella M, et al. Preclinical Targeting of Human Acute Myeloid Leukemia and Myeloablation Using Chimeric Antigen Receptor-Modified T Cells. *Blood*. 2014;123(15):2343-2354.
2. Tasian SK, Kenderian SS, Shen F, et al. Optimized Depletion of Chimeric Antigen Receptor T Cells in Murine Xenograft Models of Human Acute Myeloid Leukemia. *Blood*. 2017;129(17):2395-2407.
3. Maude SL, Tasian SK, Vincent T, et al. Targeting Jak1/2 and Mtor in Murine Xenograft Models of Ph-Like Acute Lymphoblastic Leukemia. *Blood*. 2012;120(17):3510-3518.
4. Tasian SK, Doral MY, Borowitz MJ, et al. Aberrant Stat5 and Pi3k/Mtor Pathway Signaling Occurs in Human Crlf2-Rearranged B-Precursor Acute Lymphoblastic Leukemia. *Blood*. 2012;120(4):833-842.
5. Tasian SK, Hurtz C, Wertheim GB, et al. High Incidence of Philadelphia Chromosome-Like Acute Lymphoblastic Leukemia in Older Adults with B-All. *Leukemia*. 2017;31(4):981-984.
6. Tasian SK, Teachey DT, Li Y, et al. Potent Efficacy of Combined Pi3k/Mtor and Jak or Abl Inhibition in Murine Xenograft Models of Ph-Like Acute Lymphoblastic Leukemia. *Blood*. 2017;129(2):177-187.
7. Sharman J, Hawkins M, Kolibaba K, et al. An Open-Label Phase 2 Trial of Entospletinib (Gs-9973), a Selective Spleen Tyrosine Kinase Inhibitor, in Chronic Lymphocytic Leukemia. *Blood*. 2015;125(15):2336-2343.
8. Ritchie ME, Phipson B, Wu D, et al. Limma Powers Differential Expression Analyses for Rna-Sequencing and Microarray Studies. *Nucleic Acids Res*. 2015;43(7):e47.

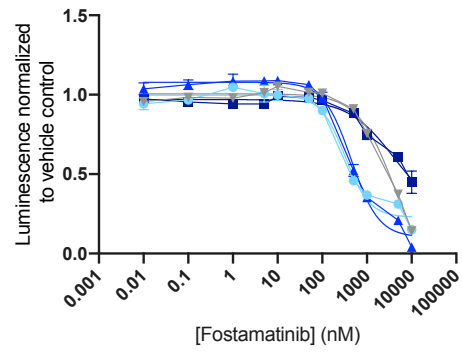
# Supplemental Figure 1

**A**



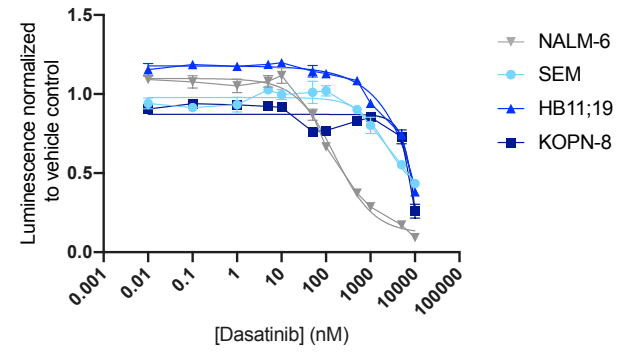
	NALM-6	SEM	HB11;19	KOPN-8
IC50	303.1	542.4	226.4	~ 1904755

**B**



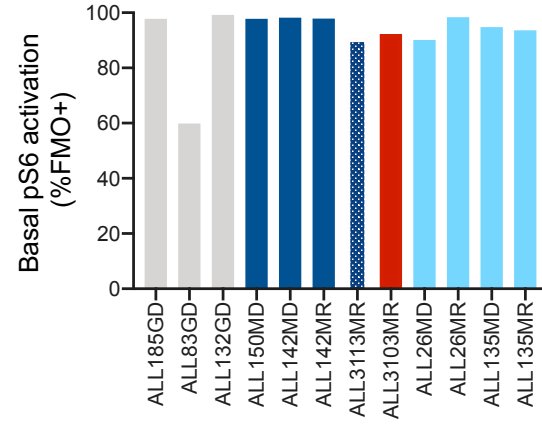
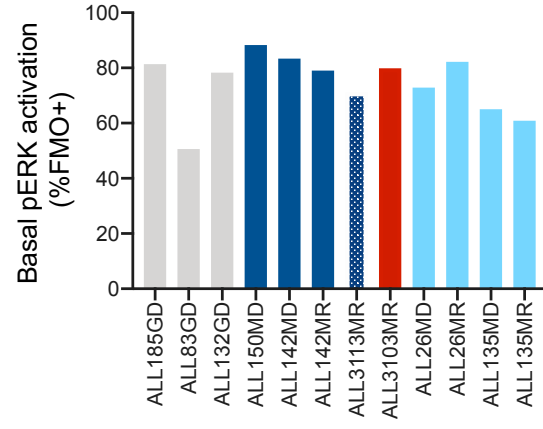
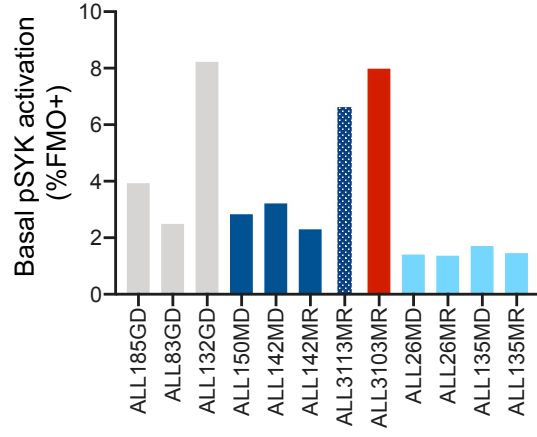
	NALM-6	SEM	HB11;19	KOPN-8
IC50	4312	323.4	445.8	4039

**C**

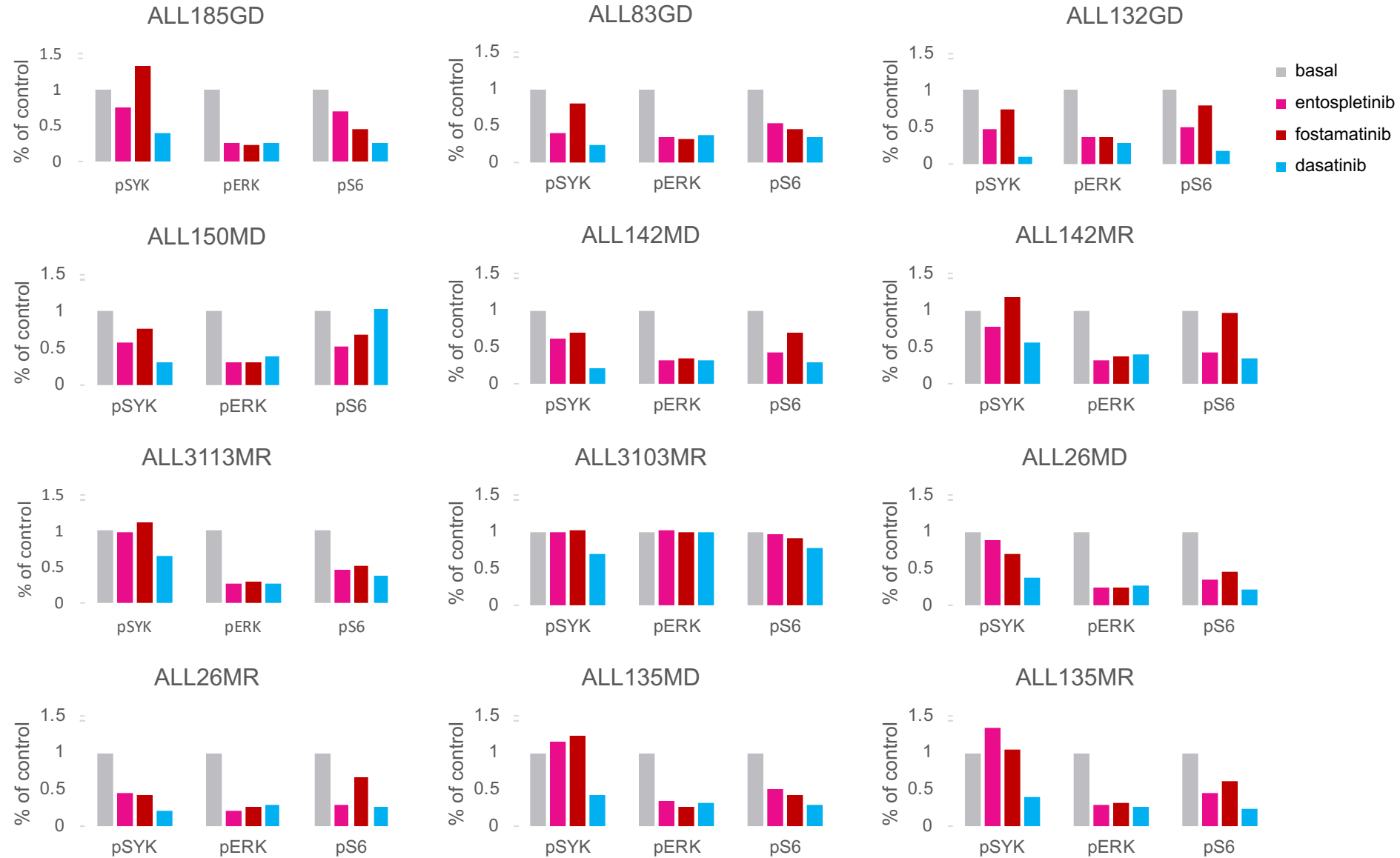


	NALM-6	SEM	HB11;19	KOPN-8
IC50	159.7	2364	~ 18512275	~ 38999

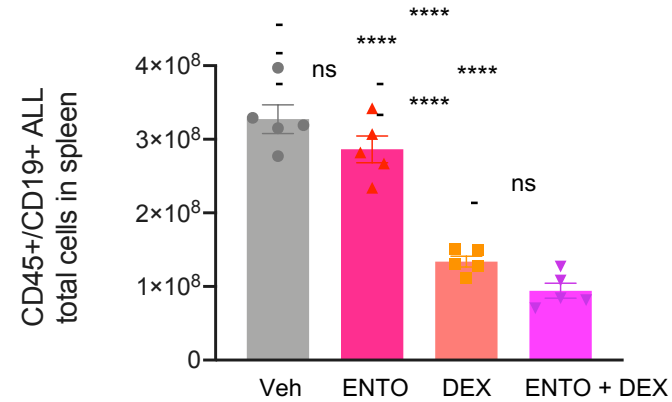
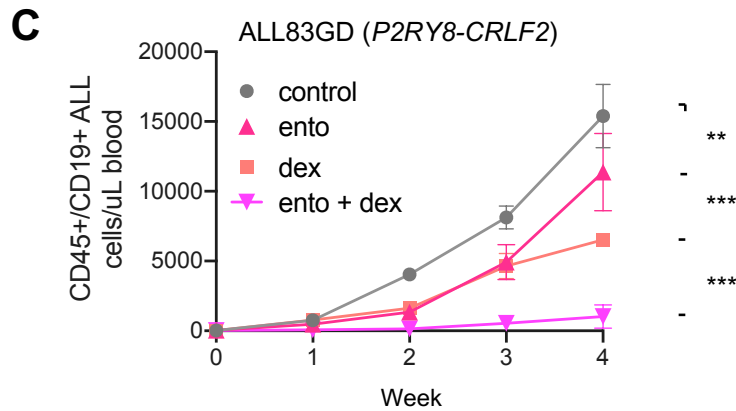
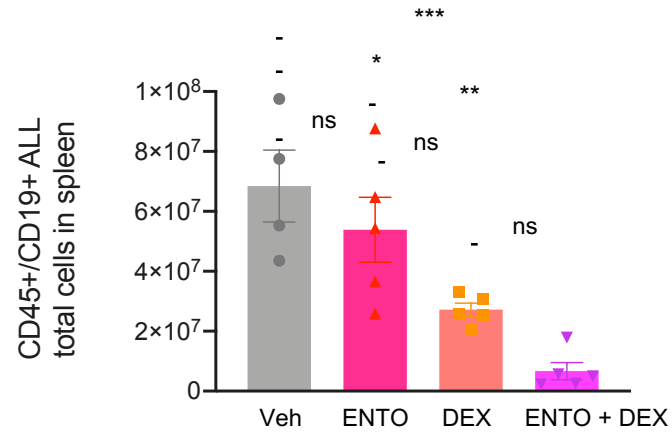
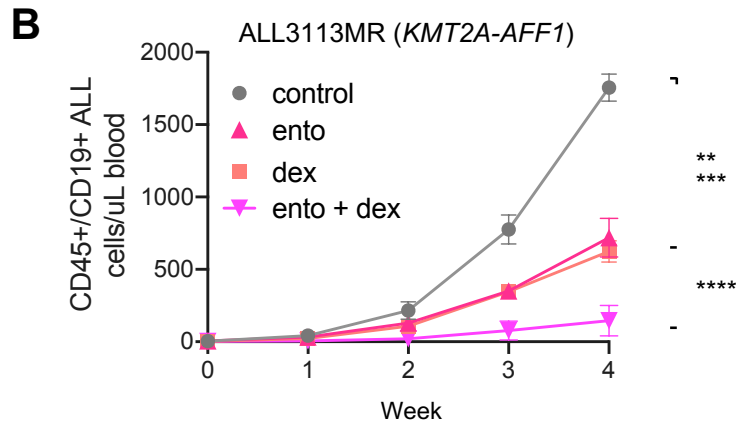
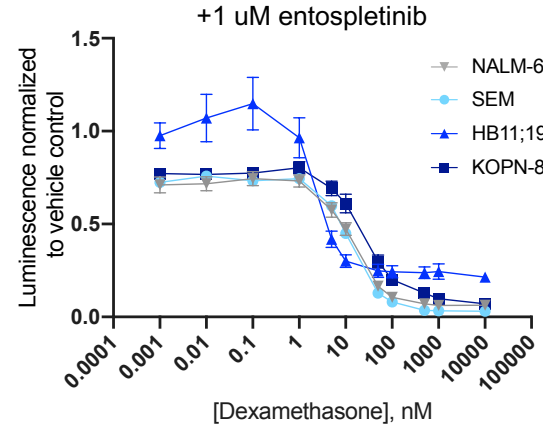
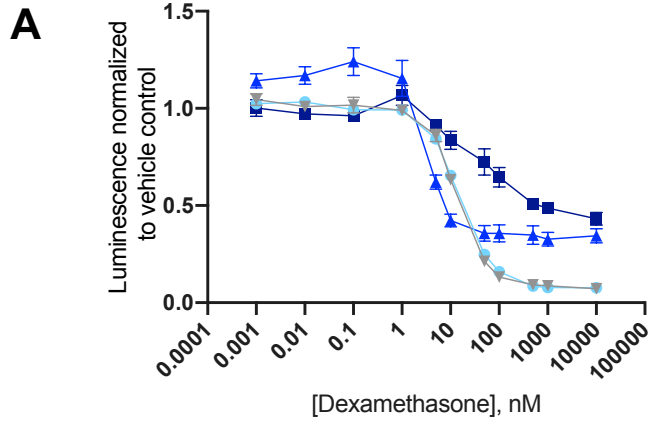
# Supplemental Figure 2



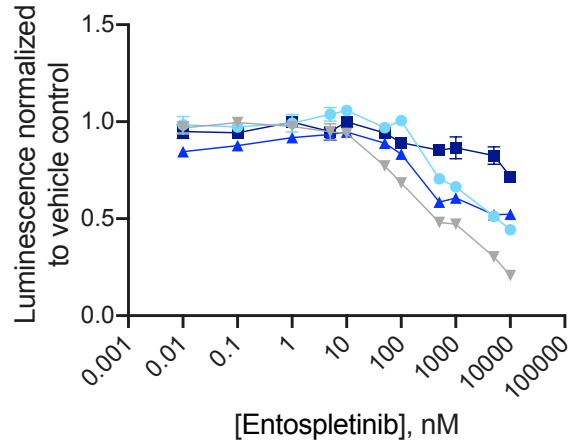
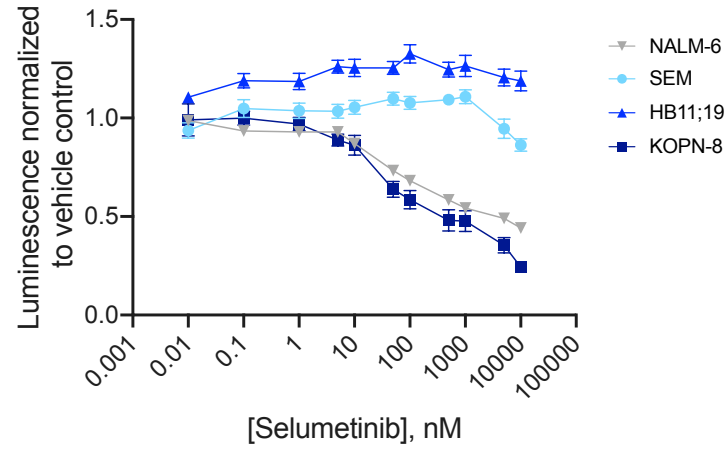
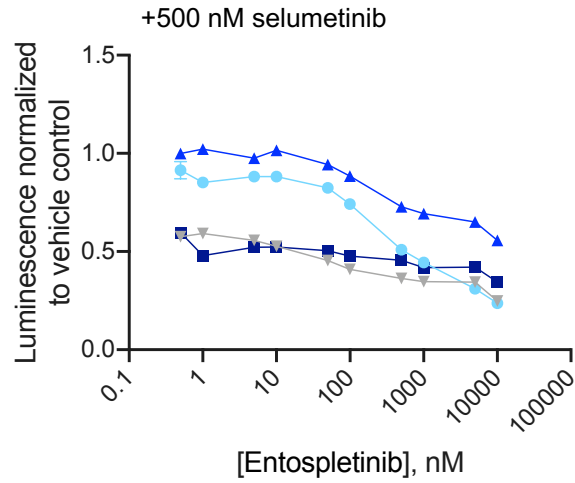
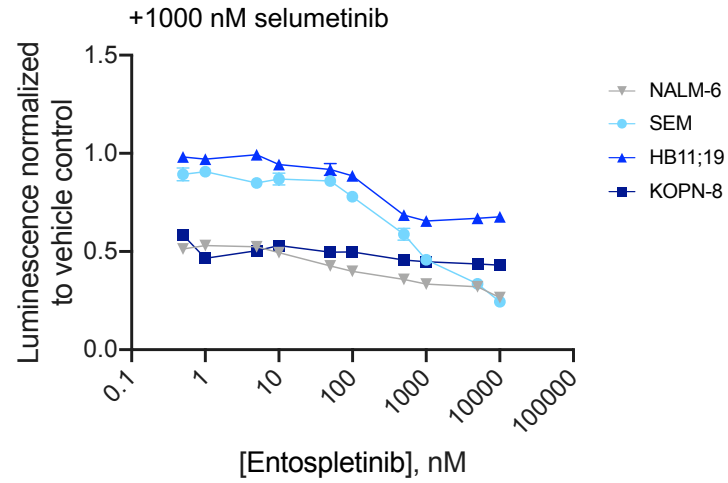
# Supplemental Figure 3



# Supplemental Figure 4

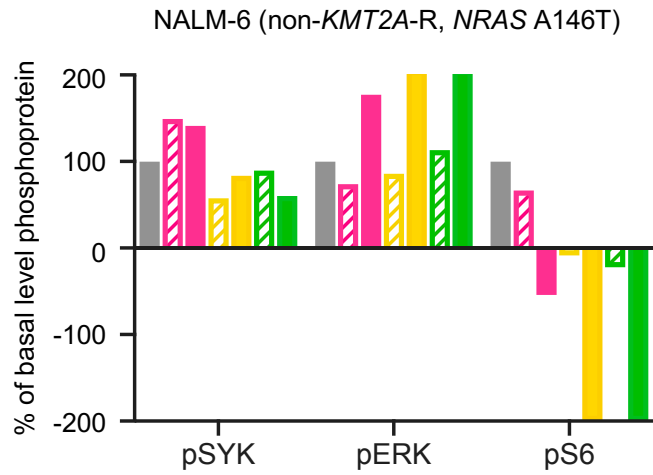


# Supplemental Figure 5

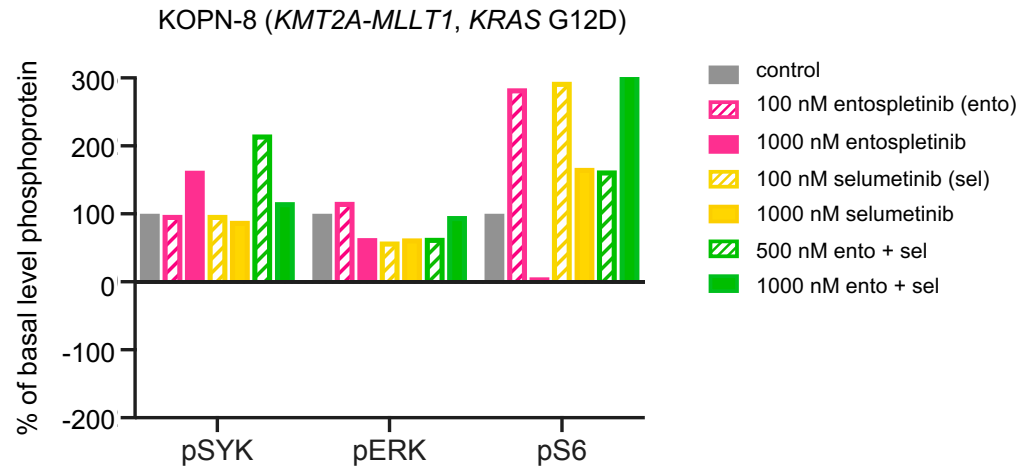
**A****B****C****D**

# Supplemental Figure 6

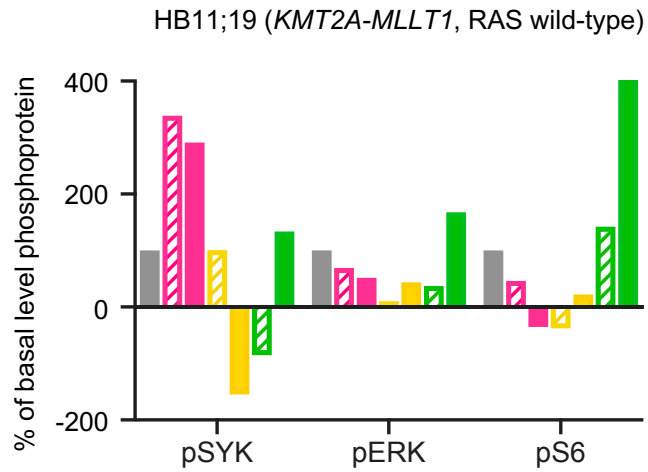
**A**



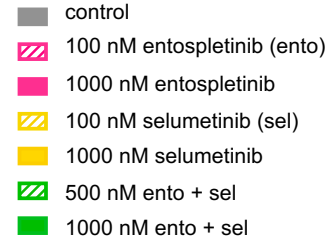
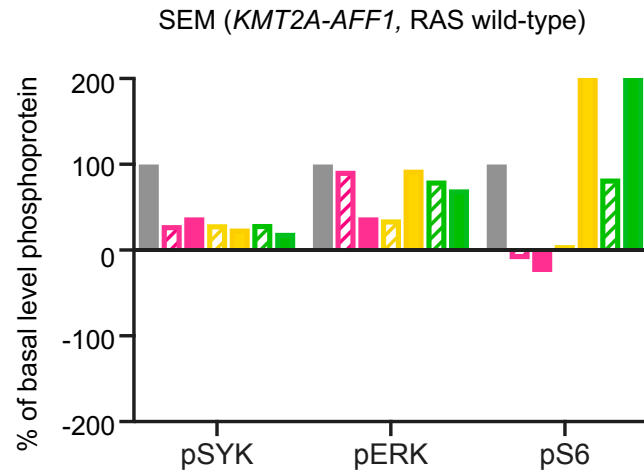
**B**



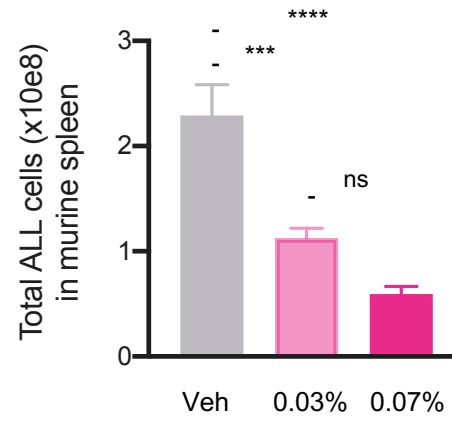
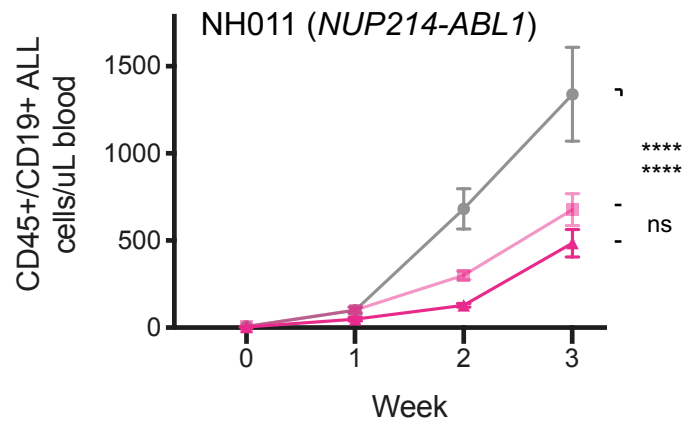
**C**



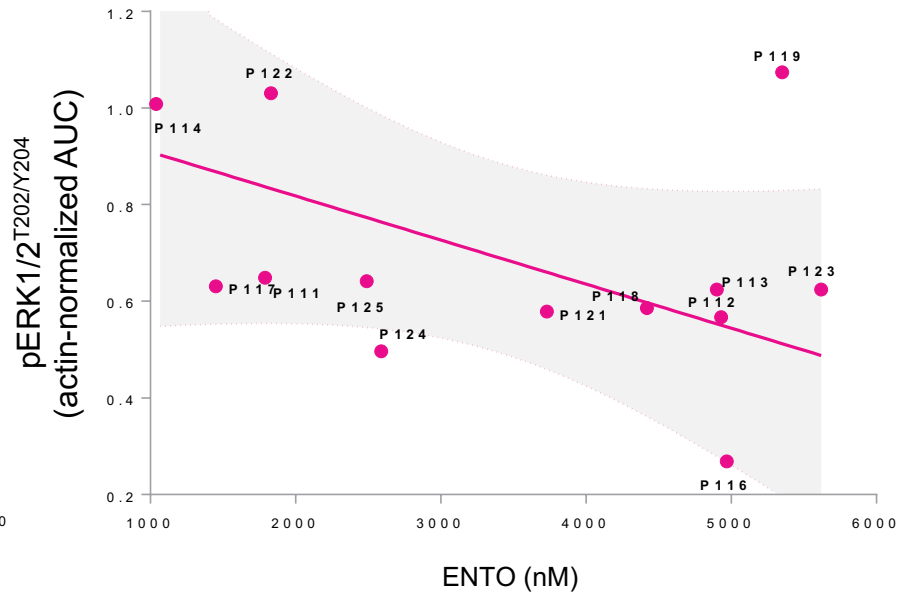
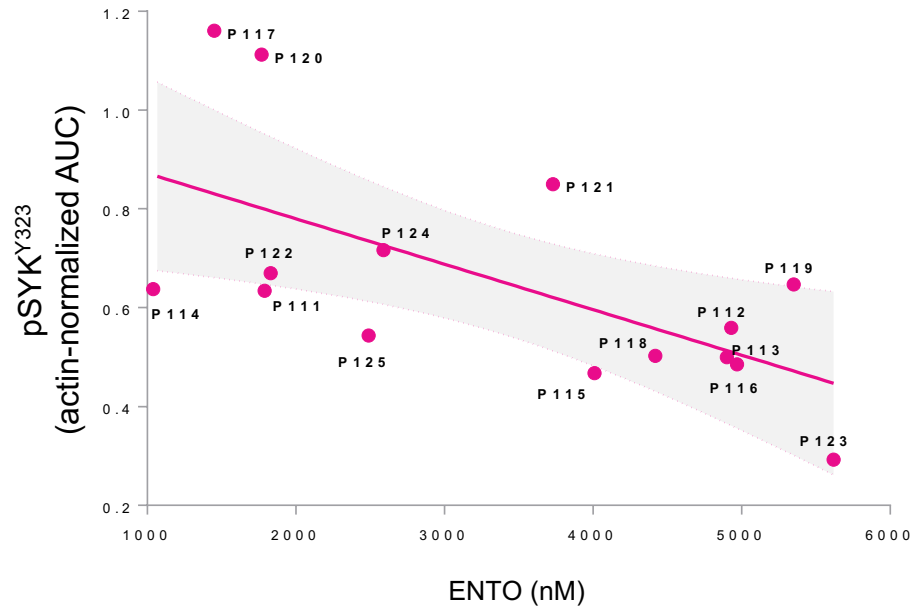
**D**



# Supplemental Figure 7

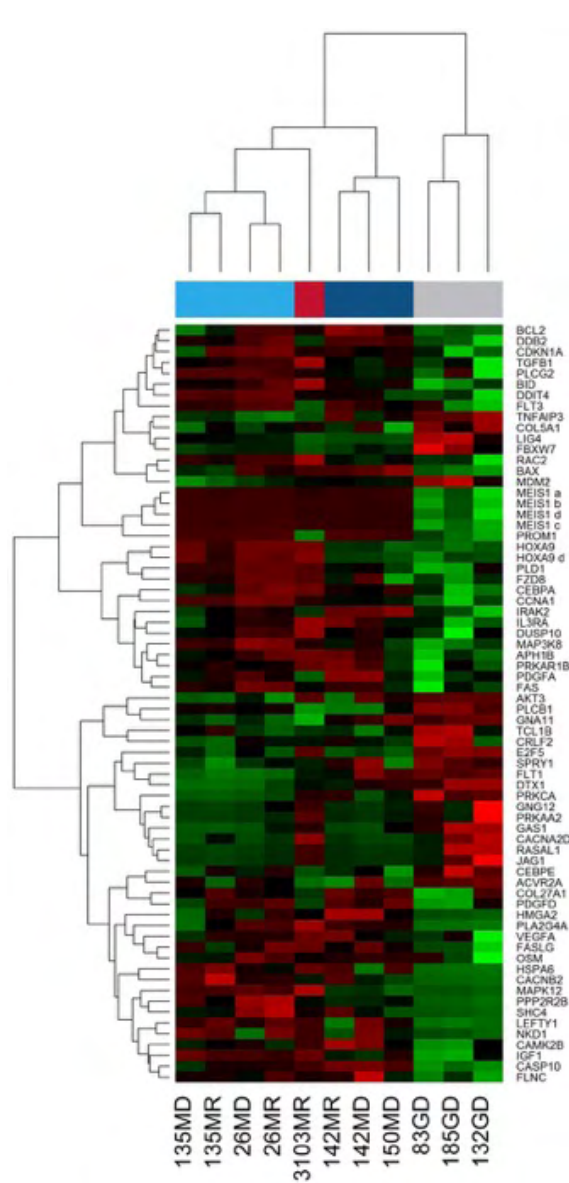


# Supplemental Figure 8

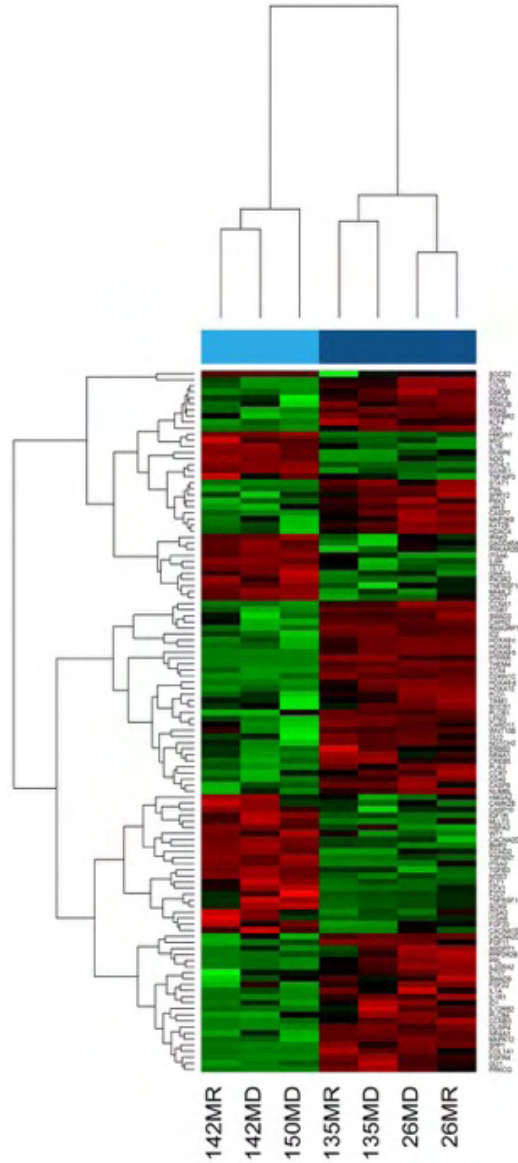


# Supplemental Figure 9

**A** *KMT2A-R* vs non-*KMT2A-R*



**B** *KMT2A-AFF1* vs *KMT2A-MLLT1*



# Supplemental Figure 10

